Thermal Performance Enhancement of Lithium-Ion Batteries Using Phase Change Material

by

Sarmad Ali

A thesis submitted in partial fulfillment for the
degree of Master of Science

in the

Faculty of Engineering

Department of Mechanical Engineering

2024

I dedicate this thesis to my beloved parents, my sister, and my esteemed supervisor, whose unwavering support and encouragement have been the cornerstone of my journey through the pursuit of my Master's Degree.

CERTIFICATE OF APPROVAL

Thermal Performance Enhancement of Lithium-Ion Batteries Using Phase Change Material

by

Sarmad Ali

(MME223006)

THESIS EXAMINING COMMITTEE

S. No.	Examiner	Name	Organization
(a)	External Examiner	Dr. Naseem Ahmed	IST, Islamabad
(b)	Internal Examiner	Dr. Muhammad Irfan	CUST, Islamabad
(c)	Supervisor	Dr. M. Mahabat Khan	CUST, Islamabad

Dr. M. Mahabat Khan
Thesis Supervisor
April, 2024

Dr. M. Mahabat Khan
Head
Dept. of Mechanical Engineering
April, 2024

Dr. Imtiaz Ahmad Taj
Dean
Faculty of Engineering
April, 2024

Author's Declaration

I, **Sarmad Ali** hereby state that my MS thesis titled "**Thermal Performance Enhancement of Lithium-Ion Batteries Using Phase Change Material**" is my own work and has not been submitted previously by me for taking any degree from Capital University of Science and Technology, Islamabad or anywhere else in the country/abroad.

At any time if my statement is found to be incorrect even after my graduation, the University has the right to withdraw my MS Degree.

(Sarmad Ali)

Registration No: MME223006

Plagiarism Undertaking

I solemnly declare that research work presented in this thesis titled "**Thermal Performance Enhancement of Lithium-Ion Batteries Using Phase Change Material**" is solely my research work with no significant contribution from any other person. Small contribution/help wherever taken has been duly acknowledged and that complete thesis has been written by me.

I understand the zero tolerance policy of the HEC and Capital University of Science and Technology towards plagiarism. Therefore, I as an author of the above titled thesis declare that no portion of my thesis has been plagiarized and any material used as reference is properly referred/cited.

I undertake that if I am found guilty of any formal plagiarism in the above titled thesis even after award of MS Degree, the University reserves the right to withdraw/revoke my MS degree and that HEC and the University have the right to publish my name on the HEC/University website on which names of students are placed who submitted plagiarized work.

(Sarmad Ali)

Registration No: MME223006

List of Publications

It is certified that following publication(s) have been made out of the research work that has been carried out for this thesis:-

1. **Sarmad Ali**, M. M. Khan, "Experimental Investigation of Battery Thermal Management System of Lithium-Ion Cells Using PCM," *Eng. Proc. 2023, 45(1), 52; https://doi.org/10.3390/engproc2023045052.*

2. **Sarmad Ali**, M. M. Khan, M. Irfan, "Thermal Performance Enhancement of Lithium-Ion Batteries Using Phase Change Material and Fin Geometry Modification" *World Electr. Veh. J. 2024, 15(2), 42; https://doi.org/10.3390/wevj15020042*

(Sarmad Ali)

Registration No: MME223006

Acknowledgement

I am deeply grateful to my parents and my sister, whose unwavering love, support, and encouragement have been the bedrock of my academic journey. Their belief in me has been a constant source of strength, and without their presence, none of my achievements would have been possible.

I extend my heartfelt appreciation to my supervisor, Dr. Muhammad Mahabat Khan, whose guidance and support have been invaluable throughout this research endeavor. Dr. Khan's insightful feedback and unwavering encouragement have not only enhanced the quality of my work but also enriched my understanding of the subject matter. I am truly fortunate to have had the opportunity to learn under his mentorship.

Additionally, I would like to express my gratitude to Dr. Muhammad Irfan for his invaluable guidance, unwavering support, and critical reviews, which have played a pivotal role in shaping this research. His expertise and constructive criticism have challenged me to strive for excellence and have significantly contributed to the completion of this study.

I am also thankful to all the faculty members and staff who have supported me throughout my academic journey. Their dedication and commitment to nurturing intellectual growth have been instrumental in shaping my academic pursuits.

Finally, I extend my appreciation to all my friends and colleagues who have provided encouragement, assistance, and camaraderie along the way. Their companionship has made this journey all the more rewarding.

(Sarmad Ali)

Abstract

The rapid increase in emissions and the depletion of fossil fuels have led to a rapid rise in the electric vehicles (EVs) industry. Electric vehicles predominantly rely on lithium-ion batteries (LIBs) to power their electric motors. However, the charging and discharging processes of LIB packs generate heat, resulting in a significant decline in the battery performance of EVs. Consequently, there is a pressing need for an effective Battery Thermal Management System (BTMS) for lithium-ion batteries in EVs. In this current study, a novel experimental BTMS is developed for thermal performance enhancement of LIB pack comprising 2x2 cells. Three distinct fin configurations (circular, rectangular, and tapered) are integrated with the outer wall of the lithium-ion cells. Additionally, the cells are fully submerged in Phase Change Material (PCM). The study considers 1C, 2C, and 3C cell discharge rates. The combination of rectangular fins and PCM manifests superior performance, reducing the mean cell temperature by 29.71%, and 28.36% as compared to unfinned lithium-ion cells under ambient conditions at 1C, and 2C discharge rates. Furthermore, at 3C discharge rate, lithium-ion cells equipped with rectangular fins demonstrate a delay of 40 minutes in reaching the maximum surface temperature of $40°C$ as compared to the unfinned ambient case. After 60 minutes of battery discharge at a 3C rate, the cell surface temperature of the rectangular fin case only reaches $42.7°C$. Furthermore, the numerical simulations show that Nusselt numbers for lithium-ion cells with rectangular fins improve by 9.72% as compared to unfinned configurations at 3C discharge rate.

Contents

List of Figures

List of Tables

Abbreviations

BTMS   Battery Thermal Managament System

LIB   Lithium-Ion Battery

PCM   Phase Change Material

Symbols

g	acceleration due to gravity	m/s^2
u	velocity	m/s
ρ	density	kg/m^3
μ	viscosity	$kg/m.s$
p	Pressure	N/m^2
h	Enthalpy	$J/kg.K$

Chapter 1

Introduction

1.1 Battery Thermal Management System

Battery Thermal Management Systems (BTMS) are indispensable in the realm of lithium-ion batteries, especially within the context of Electric Vehicles (EVs). The intricacies of EV applications, marked by high power demands and diverse operating conditions, underscore the critical role of effective thermal management in optimizing battery performance and safety. Lithium-ion batteries exhibit sensitivity to temperature fluctuations, and without proper thermal control, efficiency and longevity can be compromised, leading to potential safety hazards.

BTMS emerges as a comprehensive solution, employing advanced cooling and heating mechanisms to uphold batteries within an optimal temperature range. In addition with liquid cooling, the incorporation of phase change materials (PCMs) is gaining prominence. PCMs leverage latent heat during phase transitions to regulate temperature, offering an additional layer of thermal stability during demanding usage scenarios.

The innovation of fin geometry modification adds another dimension to BTMS efficiency. Through the optimization of heat-dissipating fins within the battery pack, engineers can elevate heat transfer rates, fostering improved thermal performance. This optimization proves pivotal in preventing temperature irregularities, safeguarding battery life and overall safety.

The evolution of BTMS not only enhances performance but also contributes substantially to the longevity and safety of lithium-ion batteries in EVs. With the continuous rise in demand for electric vehicles, ongoing research and advancements in battery thermal management will remain integral in propelling the capabilities of EV technology.

One particularly noteworthy advancement in Battery Thermal Management Systems (BTMS) involves the integration of Phase Change Materials (PCMs). PCM-based BTMS represents a cutting-edge solution that leverages the unique properties of these materials to enhance thermal regulation. PCMs undergo phase transitions, changing from solid to liquid or vice versa, and during these transitions, they absorb or release latent heat. This remarkable ability allows PCMs to act as thermal buffers, effectively mitigating temperature fluctuations within the battery pack. When strategically embedded within the battery system, PCMs play a crucial role in stabilizing temperature profiles. During periods of high demand, such as rapid charging or discharging, the PCM absorbs excess heat, preventing the battery from overheating. Conversely, during periods of low demand, the PCM releases stored heat, ensuring that the battery remains within the optimal temperature range for efficient operation. This PCM-based approach not only enhances thermal management but also contributes to the overall efficiency and longevity of lithium-ion batteries. By mitigating temperature extremes, PCM-based BTMS helps minimize thermal stress on battery components, reducing the likelihood of degradation and extending the lifespan of the battery pack. As the electric vehicle landscape continues to evolve, PCM-based BTMS stands out as a pivotal technology, pushing the boundaries of thermal management and reinforcing the reliability of lithium-ion batteries in the demanding context of electric mobility.

1.1.1 Types of Battery Thermal Management Systems

1.1.1.1 Liquid Cooling Systems

Liquid cooling systems are a widely employed BTMS, utilizing a circulating coolant to absorb and dissipate heat generated during charging and discharging cycles. The

coolant flows through dedicated channels within the battery pack, effectively regulating temperature and maintaining a stable operational environment for lithium-ion cells.

1.1.1.2   Forced Air Cooling Systems

Forced air cooling systems employ fans or blowers to actively circulate air across the battery pack. This method enhances heat dissipation by increasing the airflow, making it particularly effective in scenarios where natural convection may be insufficient. Forced air cooling is a cost-effective solution and is often used in conjunction with other cooling methods for improved thermal management.

1.1.1.3   Hybrid Cooling Systems

Hybrid cooling systems combine two or more cooling methods to optimize thermal management. For example, a hybrid system may integrate liquid cooling and forced air cooling to leverage the benefits of both methods. This approach allows for greater flexibility in adapting to varying operating conditions, providing efficient heat dissipation across a wide range of scenarios.

Hybrid cooling systems aim to achieve a balance between performance, cost, and energy efficiency in battery thermal management.

1.1.1.4   Phase Change Material (PCM) Based Systems

PCM-based BTMS leverages the unique properties of phase change materials to enhance thermal regulation. PCMs undergo phase transitions, absorbing or releasing latent heat during these transitions. By strategically incorporating PCMs into the battery design, this system acts as a thermal buffer, absorbing excess heat during high-demand periods and releasing it during low-demand phases.

1.1.1.5   Thermal Runaway Prevention Systems

These systems focus on early detection and prevention of thermal runaway, a phenomenon where temperature spikes lead to uncontrollable and rapid heating.

Advanced sensors and control mechanisms are employed to identify potential issues and implement measures such as reducing charging rates or activating cooling systems to prevent thermal runaway.

1.1.1.6 Direct Liquid Immersion Systems

In this approach, batteries are directly immersed in a thermally conductive liquid. This method provides efficient heat dissipation due to the direct contact between the liquid and battery components. Direct liquid immersion is known for its effectiveness in managing temperature, but it requires careful design considerations to prevent leakage and ensure safety.

1.1.1.7 Active Thermal Control Systems

Active thermal control systems utilize electric heaters or coolers to actively adjust the temperature of the battery pack. This approach allows precise control over the thermal environment and is often combined with other passive cooling methods for a comprehensive and dynamic thermal management strategy.

1.2 Passive Cooling Using Phase Change Materials

Phase Change Material (PCM)-based Battery Thermal Management Systems (BTMS) have emerged as a revolutionary approach to address the thermal challenges associated with lithium-ion batteries, particularly in the context of electric vehicles (EVs). This innovative cooling method utilizes materials that undergo phase transitions, changing from solid to liquid and vice versa, while absorbing or releasing latent heat during these transitions. The fundamental principle behind PCM-based BTMS is to leverage the latent heat absorption or release during the phase change of the material. PCMs have a distinct advantage in their ability to absorb a significant amount of heat without a substantial increase in temperature, providing an effective means of temperature regulation within the battery pack.

This property allows PCMs to act as thermal buffers, absorbing excess heat during high-demand situations, such as rapid charging or discharging, and releasing it during low-demand periods. The integration of PCM into the battery design introduces a dynamic and adaptive thermal management system. During periods of intense battery activity, the PCM absorbs heat and undergoes a phase change, preventing the temperature from rising sharply.

Conversely, during periods of low activity, the PCM releases stored heat, maintaining the battery within the optimal temperature range for efficient operation. One of the notable advantages of PCM-based BTMS is its ability to mitigate thermal runaway risks. Thermal runaway, a phenomenon characterized by uncontrolled and rapid temperature increase, poses a significant safety concern for lithium-ion batteries. PCM's ability to absorb and distribute heat evenly helps prevent localized hotspots, reducing the likelihood of thermal runaway events.

Additionally, PCM-based BTMS contributes to the overall longevity of lithium-ion batteries. By minimizing thermal stress on battery components, this cooling method helps alleviate degradation, extending the lifespan of the battery pack. This not only enhances the economic viability of electric vehicles but also aligns with sustainability goals by promoting longer-lasting energy storage solutions. PCM-based BTMS represents a promising avenue for advancing the efficiency, safety, and longevity of lithium-ion batteries in electric vehicles. The dynamic nature of PCM allows for precise thermal regulation, making it a key player in the evolution of battery technology for the sustainable future of electric mobility.

1.3   PCMs and Their Types

Phase Change materials are substances capable of undergoing phase transitions, typically changing from solid to liquid and vice versa, while absorbing or releasing latent heat. This unique property makes them ideal for thermal energy storage and regulation in Battery Thermal Management Systems (BTMS). Following are the types of Phase Change Materials PCMs:

1.3.1 Organic PCMs

Organic PCMs are derived from hydrocarbons, fatty acids, or paraffins. They are known for their diverse range of phase change temperatures, making them adaptable to specific thermal requirements. Organic PCMs often exhibit high latent heat capacity, providing efficient energy storage during phase transitions.

1.3.2 Inorganic PCMs

Inorganic PCMs are based on salts, metals, or other inorganic compounds. These materials offer high thermal conductivity and stability, making them suitable for applications where precise temperature control is critical. Inorganic PCMs are less prone to degradation over repeated phase transitions, ensuring long-term reliability.

1.3.3 Bio-based PCMs

Bio-based PCMs are sourced from renewable materials such as natural oils or fats. They provide an environmentally friendly alternative, aligning with sustainability goals. Bio-based PCMs offer thermal properties comparable to traditional PCMs while reducing reliance on non-renewable resources.

1.3.4 Eutectic PCMs

Eutectic PCMs consist of a mixture of two or more substances that, when combined in specific ratios, create a blend with a single, well-defined melting point. This characteristic ensures a sharp and predictable phase change, enhancing the precision of thermal regulation in BTMS applications.

1.3.5 Micro Encapsulated PCMs

Micro encapsulated PCMs involve enclosing PCM particles within microscopic capsules. This encapsulation provides controlled release of latent heat, improving

compatibility with various materials and facilitating the integration of PCMs into battery systems. The micro encapsulation process enhances stability and prevents PCM leakage. Following Figure 1.1 shows the classification of PCMs [1]
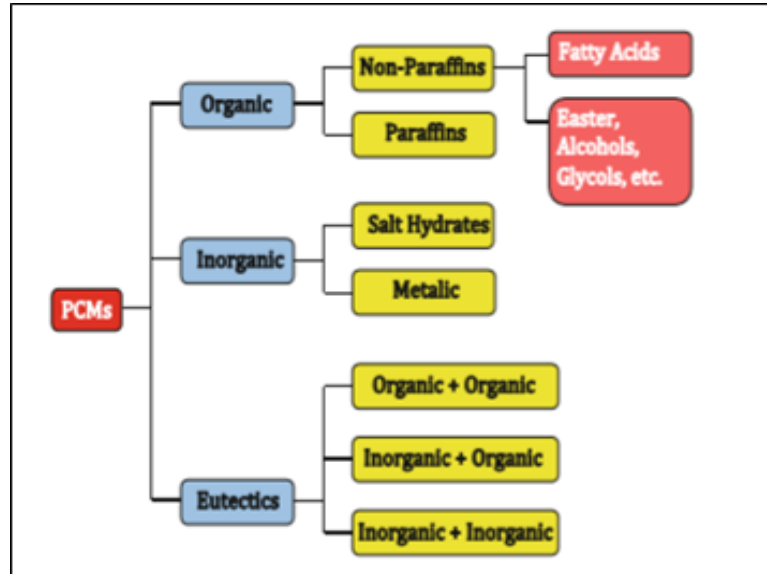
FIGURE 1.1: Classification of PCMs and sub classes for organic in organic and eutectic PCMs. [1]

1.4 Scope of the Study

1.4.1 Development of a Novel Lithium-Ion Cell Tester

1. Design and implementation of a state-of-the-art lithium-ion cell tester.

2. Focus on accuracy, precision, and versatility to ensure comprehensive cell characterization. Battery Pack Development for Testing

1.4.2 Battery Pack Development for Testing

1. Design and construction of a dedicated battery pack for testing purposes which included different fins and unfinned LIB packs

2. Consideration of real-world conditions, ensuring the pack simulates practical scenarios for accurate assessments.

1.4.3 Experimental Phase

1. Rigorous experimentation using the developed cell tester and battery pack.

2. Comprehensive testing of lithium-ion cells to gather data on performance, efficiency, and behavior under various operating conditions.

1.4.4 CFD Numerical Comparison

1. Integration of Computational Fluid Dynamics (CFD) simulations for a numerical comparison.

2. Utilization of advanced modeling techniques to analyze and predict thermal behavior within the battery pack.

1.4.5 Thermal Performance Parameters Testing

1. Evaluation of thermal performance parameters, including temperature distribution, heat dissipation, and overall heat management.

2. Comparison of experimental results with CFD simulations to validate the accuracy of the numerical model.

1.4.6 Analysis and Interpretation

1. In-depth analysis of experimental and numerical data to draw correlations and identify trends.

2. Interpretation of results to understand the impact of various factors on thermal performance.

1.4.7 Conclusions and Future Directions

1. Summarize key findings and their implications for the field of battery technology.

2. Suggest potential avenues for future research and development, building on the insights gained from the study.

1.5 Thesis overview

This thesis comprises of an abstract and 6 chapters, details of which are as follow:

1. **Introduction** is the current chapter which explains the background of this research and the scope of this study. Prior to this section the Abstract and different terminologies have been explained.

2. **Literature Review** followed by introduction, a detailed literature review is discussed with backgrounds to emissions of conventional internal combustion vehicles which leads to developments of EVs. Details of previously studied Battery Thermal Managment Systems have been discussed in detail.

3. **Experimental Setup** chapter discusses the development of the experimental test rig which includes the manufacturing of LIB pack and the novel controller circuit for battery testing. The details of the sensors and data acquisition systems is also discussed.

4. **Numerical Methodology** All the details of domain discretization and numerical methods used along with their equations are discussed in detail. Time step and mesh independence study is also discussed in this section.

5. **Results and Discussion** This is a detailed section in which the firstly the experimental results are discussed which then leads to the numerical validation and comparison of numerical results with the experimental results. Thermal perfomance parameters are also discussed.

6. **Conclusion** A summarized details of the enhancements achieved and the results are discussed relating to all the parametric variations in this research.

Chapter 2

Literature Review

Concerns about the environment and the need for zero-emission transportation have pushed for the development of electric vehicles (EVs) [2]. The growth of the electric vehicle (EV) market was catalysed by the increased public awareness of climate change and the necessity for clean energy. Electric vehicles (EVs) have emerged as the most promising mode of transportation due to their minimal operational costs, high speed, and energy-efficient battery technologies [3].

According to Quadrelli and Peterson CO_2 emissions play a great role in the increased green house gasses and inturn result in overall temperature rise. The effects of rising greenhouse gas concentrations may take time to manifest due to system inertia in climate, ecology, and socio-economic interactions. Pollution resulting from traditionally powered transportation vehicles can be effectively minimised by utilising cars equipped with lithium-ion batteries. Battery temperature during operation is an important element that affects battery life [4–6]. Even after stabilizing CO_2 levels, surface temperature will continue to rise for over a century, and sea levels will persistently increase for many centuries. Certain climate changes are essentially irreversible due to the internal combustion engines. Figure 2.1 shows the rise in temperature over the past century with predictions for the next 10 centuries [7].

In China, battery electric vehicles and plug-in hybrid electric vehicles save energy and emit less CO_2 than regular petrol ICEVs. Variations are noted among regional

grids, with greater benefits in the Central, South, Northwest, and Hainan Power systems. In contrast, North, Northeast, and East China power grids show lesser savings due to a higher amount of coal-fired power [8] as shown in Figure 2.2.
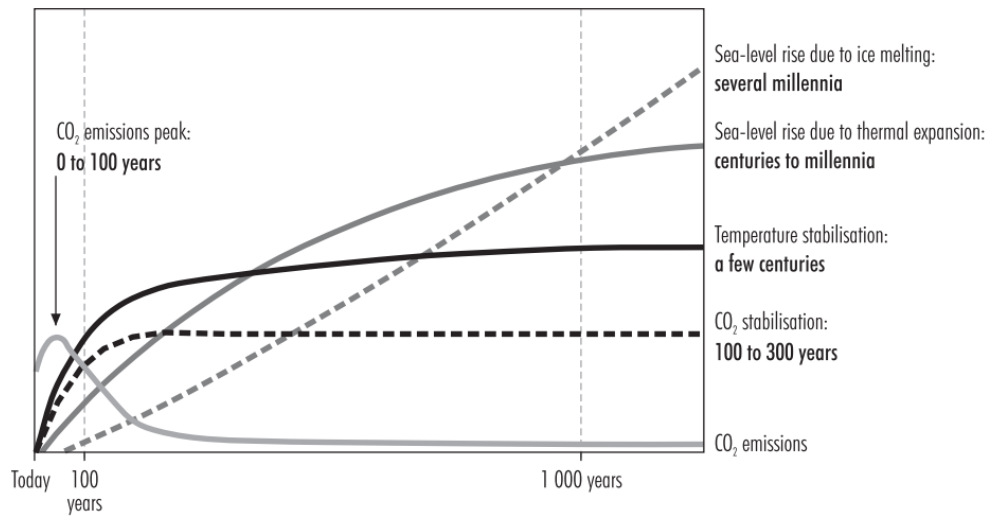
FIGURE 2.1: Timeframes for climate change impacts (generic representation for stabilizing CO_2 concentration at any level between 450 and 1000 parts per million by volume (ppmv)) [7].

In China, battery electric vehicles and plug-in hybrid electric vehicles save energy and emit less CO_2 than regular petrol ICEVs. Variations are noted among regional grids, with greater benefits in the Central, South, Northwest, and Hainan Power systems.

In contrast, North, Northeast, and East China power grids show lesser savings due to a higher amount of coal-fired power [8] as shown in Figure 2.2.
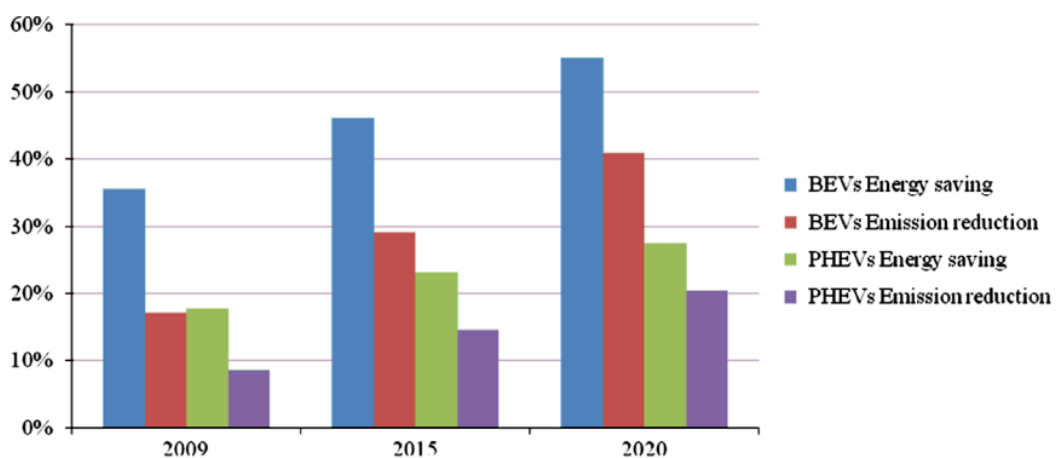
FIGURE 2.2: BEVs and PHEVs savings in emissions over China [8]

In comparison to other popular rechargeable batteries such as Nickle-Cadmium, Ni-Metal hydride, and Lead-acid batteries, the Lithium-Ion battery has a high energy and power density, a long service life, and is environmentally friendly, and has thus been widely used in consumer electronics [9]. Because of their durability, extended cycle life [10] low self-discharge rate, and large capacity [11], lithium-ion batteries are primarily declared as power source of Electric vehicles. Figure 2.3 shows the setup used for the testing of Li-Ion Cell.
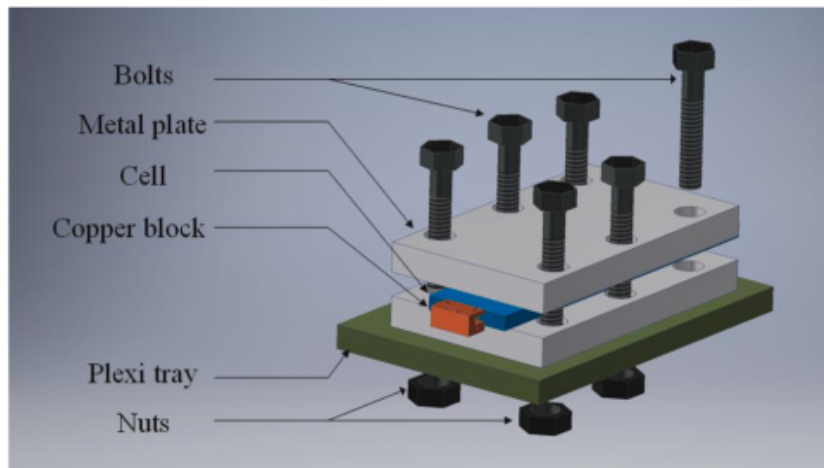
FIGURE 2.3: Physical test bench for each cell in this study [10].

The primary difficulties for the battery are heat and severe temperatures, which can occur at high discharge rates during scenarios such as rapid acceleration [12]. To maintain equal temperature distribution among the cells, an effective BTMS is necessary [13]. According to patel et al. [13] the shift to electric vehicles (EVs) poses a substantial problem because lithium-ion batteries' efficiency is temperature dependent.

A reliable battery thermal management system (BTMS) is required. The authors examined active and passive BTMS, with a focus on passive solutions such as Phase Change Material (PCM) and heat pipes. PCM and heat pipe-based BTMS are effective without increasing power usage. Hybrid BTMS, which combines active and passive parts, provides greater thermal regulation.

The statistical study reveals improvements in maximum battery temperature and temperature differential. The essay focuses on establishing practical and cost-effective BTMS solutions within power, volume, and weight constraints [14].
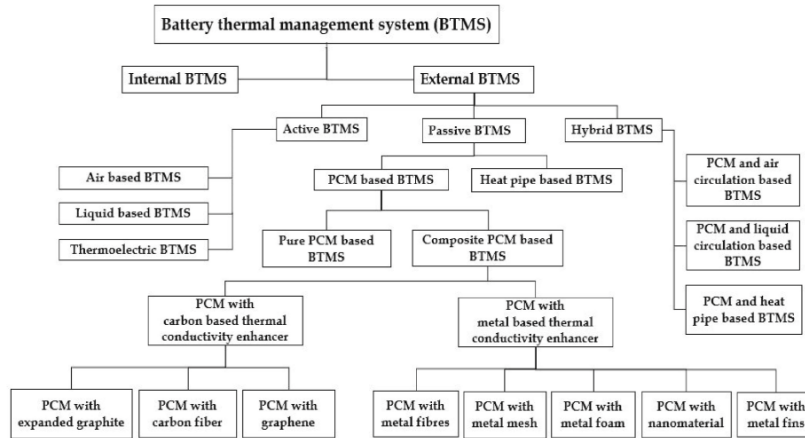
FIGURE 2.4: A detailed BTMS classification [14].

To address all of these requirements, research studies on the BTMS have been conducted using several mediums for heat transfer such as air, liquid and PCM-based cooling [15–19]. Lin et al. [20] investigated a temperature range of $-10°C$ to $50°C$ has been identified as an optimum temperature range for a lithium-ion battery. However, observations showed that the Lithium Ion batteries perform optimally between $20 - 40°C$ [21].

Motloch et al. [22] investigated that in an operating temperature $30 - 40°C$ range, every $1°C$ rise in temperature reduced the lifetime of a battery by two months approximately. An optimal Li-Ion battery operation can be done by maintaining battery temperature within safe limits. There are several ways to control these temperatures, including liquid cooling [23], air cooling [24], and passive cooling with phase change materials.

Park and Jung [25] conducted a numerical analysis to examine the cooling efficiency of lithium-ion batteries using different cell configurations and heat transfer fluid types. It was discovered that air cooling was most effective for the larger battery design with a small gap between cells, whereas liquid cooling was more suitable for the narrower battery design. At a high rate of discharge, the air-cooling system consumed more power compared to the liquid cooling approach. Pender-gast et al. [26] designed a water cooling system specifically for a battery module that has Panasonic 18650 cells enclosed in an aluminum case. The liquid cooling system was projected to be 3500 times more efficient than the air cooling system,

resulting in a 40% reduction in load [27]. However, this improvement in efficiency comes at the expense of increased complexity and running cost. Huo and Rao [28] conducted a simulation to evaluate the thermal efficiency of a system consisting of one battery and five batteries. The system utilised liquid cooling BTMS and the cooling medium used was either pure water or Al_2O_3-water nanofluid. The researchers discovered that adding 0.04 vol.% of Al_2O_3 resulted in a 7% decrease in the average cell temperature of batteries. This was due to the enhanced cooling capabilities compared to using pure water cooling BTMS. Al-Zareer utilized ammonia [29] and liquid propane [30] as high-temperature fluids (HTF) in the construction of BTMS. Both ammonia and liquid propane filled only 5% of the surface and were filled at a pressure of around 8.5 bars. It was observed that the rise in pressure resulted in a decrease in the temperature gradient across the surface, despite a rise in the mean surface temperature. The researchers discovered that utilizing propane and ammonia-based BTMS resulted in superior regulation of cooling on the battery's surface temperature. This method effectively kept the surface temperature below 40 °C even during extremely rapid charging and discharging at a rate of 7.5 C. Al-Hallaj et al. [31] were the first to propose BTMS based on Phase Change materials. Sabbah et al. [23] investigated Li-Ion cells by air as well as PCM-based cooling. The results showed that the ambient temperatures being high combined with a high discharge rate fail to maintain the battery temperature under safe limits. Traditional PCM-based BTMS cover the battery pack's entire empty area with PCM. However, this technique causes uneven heat rejection, with corner cells releasing heat faster than central cells, resulting in temperature differences. To solve this issue, Jilte et al. developed a unique battery arrangement [32]. This novel design comprises encasing battery cells in cylindrical blocks of PCM, as seen in Figure 2.5 The spaces between cells promote natural convection, resulting in efficient heat absorption from PCM. This BTMS arrangement exhibited outstanding temperature consistency, measuring 0.05 °C and 0.12 °C at discharge rates of 2 C and 4 C. Additionally, this structure helped to reduce the total weight of the lithium-ion battery pack. Chen et al. [33] numerically analyzed Battery TMS using air cooling as well as PCM-based cooling method. Simulations are done at various ambient temperatures, intake velocities of air cooling, and PCM phase change temperatures by applying the actual current profile

to the battery model. The results showed that the air-cooling method is cheaper than PCM cooling but in a longer life cycle, the air-cooling shows nonuniformity.
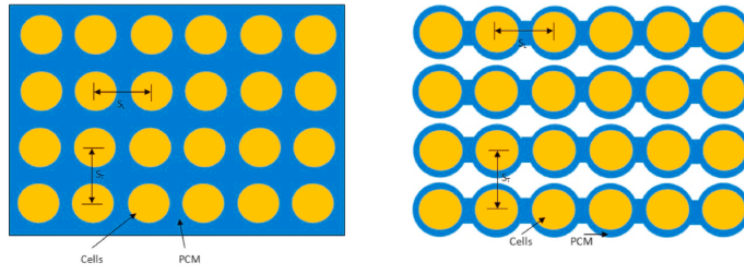
FIGURE 2.5: Side-by-side view of (a) the traditional PCM-based Battery Thermal Management System (BTMS) and (b) the adapted PCM-cooled naturally ventilated BTMS as proposed [32].

Wang et al. [34] experimentally investigated the effects of fins on battery TMS performance by using low melting temperature ($44°C$) paraffin wax. The battery temperature, on average, was lowered by $8°C$. Sun et al. [35] introduced a BMTS incorporating a CPCM and fins, featuring longitudinal cylindrical and longitudinal fins. Initial experiments were done to assess the performance of various BTMS configurations. It was deduced that the Fin-PCM composite system had the best performance as compared to the other cases at high heat generation rates of 20W. Zhao et al. [36] investigated BTMS using PCM. Copper Foam was used to eradicate the low thermally conductive PCM having thermal performance issues for temperature control. Active cooling was also done using cooling fluid running through tubes evenly distributed in the composite Phase Change Material (CPCM).

Numerical investigation was done using ANSYS Fluent by creating a BTMS model with active cooling tubes. The impact of CPCM and fluid velocity was investigated and a 14 °C lower cell temperature was seen which is a considerable improvement in thermal management employing CPCM and liquid cooling. Weng et al. [37] Investigated the effects of surrounding temperatures on BTMS. Conducting experimentations, it was found that steady-state current operations result in higher temperatures resulting in failure of a PCM-cooled BTMS and battery failure. After 1500s the at surrounding temperature of $45°C$, the battery temperatures were $54.0°C$. This led to the development of a secondary cooling system using heat pipes. Goli et al. [38] developed a composite phase change material (PCM) with

increased thermal properties by including graphene. This was done to improve the thermal management of lithium-ion batteries (LIB) due to the low thermal conductivity of PCMs.

The addition of graphene to the phase change material (PCM) resulted in a significant decrease in the temperature increase of the lithium-ion battery (LIB) module, in contrast to the standard pure paraffin. In their study, Ghadbeigi et al [39] examined the warming up capabilities of lithium-ion batteries (LIB) using two different materials: pure paraffin and a commercial phase change material (PCM) module including graphite/paraffin composites. The researchers tested the batteries under both short and extended stop situations. The findings demonstrated that the utilisation of pure paraffin, which possesses a poor thermal conductivity, provided a marginal benefit over PCM composites. This advantage was observed in terms of maintaining the LIB module at an elevated temperature and enhancing heat retention. It can be inferred that the thermal conductivity of PCM significantly affects the performance of battery thermal management.

The primary method to enhance thermal conductivity is by combining PCM with additives. However, there is insufficient information regarding the extent to which thermal conductivity can be improved. Furthermore, the specific impacts of additional factors, such as latent heat in pure phase change materials (PCM) and porosity in composite PCM, have not been thoroughly elucidated. For instance, the latent heat is a crucial factor in determining the response performance of PCM. Ramandi et al. [40] suggested the integration of two distinct phase change materials (PCM) for the purpose of regulating heat in lithium-ion batteries (LIB). A comparison was made between the effects of using one and two phase change materials (PCM) when the battery discharged at a constant rate at an average temperature of 30 ∘ C.The results demonstrated that the two-PCM configuration had a slightly higher level of efficiency compared to the one-PCM configuration. Jiang and Qu [41] devised a sandwich configuration consisting of a battery pack, phase change material (PCM), and heat pipes. The study examined many factors that affect the system, such as the melting temperature of the phase change material (PCM), the heat transfer coefficient of the heat pipes during condensation, and the thickness of the PCM. Li et al. [42] conducted an experimental study

on three systems, including natural air convection, PCM, and metal foam PCM. The study focused on a battery consisting of 9 cells discharging at current rates of 0.5C, 1C, and 3C. The previous configuration was deemed superior in terms of its ability to decrease cell temperature and achieve temperature uniformity. The comparison of battery packs with composite PCM shown a decrease in the surface temperature of the heater when compared to systems without PCM. In order to limit the increase in battery temperature to below 50 °C, a phase change material (PCM) with a melting temperature can be selected.

Nasehi et al. [43] conducted a numerical investigation on the utilisation of three layers of phase change material (PCM) to surround a battery consisting of hundred cylinder-shaped cells.In the case of under-insulated walls, a single layer configuration provides superior cooling in comparison to a three-layer design. The three-layer structure provides enhanced cooling when battery system walls are exposed to natural convection. Additionally, it was discovered that the system provides superior cooling when the phase change material (PCM) with large thermal conductivity values is filled adjacent to the battery surface.

Moraga et al. [44] conducted research on LIB pack that utilised phase change material (PCM) in either a single or triple layer configuration surrounding the battery.They investigated two distinct thicknesses: 3 mm and 12 mm. The researchers observed that out of the four phase change materials (capric acid,decahydrate sodium carbonate,octadecane,and eicosane), decahydrated sodium carbonate with a three-layer architecture resulted in a decrease in the maximum battery temperature. These findings were further validated by placing a material with strong thermal conductivity adjacent to the surface and a substance with low conductivity on the outer wall. Safdari et al. [45] analyzed BTMS using a coupled system with active cooling channels and PCM-based passive cooling of 18650 Li-Ion batteries.

The results showed that at low discharge rates, the PCM-based cooling was effective in controlling temperatures. However, at a high discharge rate, for effective cooling of the battery pack, the active air channels around the container played a major role when the passive cooling failed. Li et al. [46] conducted research

on optimization techniques with the goal of reducing the overall amount of phase change material (PCM) in cylindrical BTMS. An analysis was conducted to optimise the mass of phase change material (PCM) by examining the impact of battery diameter, spacing, PCM thickness, and heat generation rates. The temperature difference reaches a maximum value of approximately 2.9°C and 3.5°C for PCM radii of 48 mm and 55 mm, respectively.

Rao et al. [47] used a mini-channel paired with PCM-based BTMS for Li-ion batteries. Initially, the PCM absorbed the generated heat from the battery, which was subsequently discharged into the environment via liquid flowing via the mini-channel. Several parameters were investigated, including water mass flow rate, number of channels, phase change temperature, and thermal conductivity of the PCM.

The results showed that having more mini-channels resulted in a greater drop in battery temperature and better temperature uniformity. However, it was discovered that PCM-based BTMS surpasses hybrid BTMS for temperature uniformity. Optimal conditions, with eight mini-channels and a mass flow rate of 8×10^{-4} kg/s, provided a phase transition temperature of 308.15°C, thermal conductivity of 0.6 W/m-°C, and temperature.
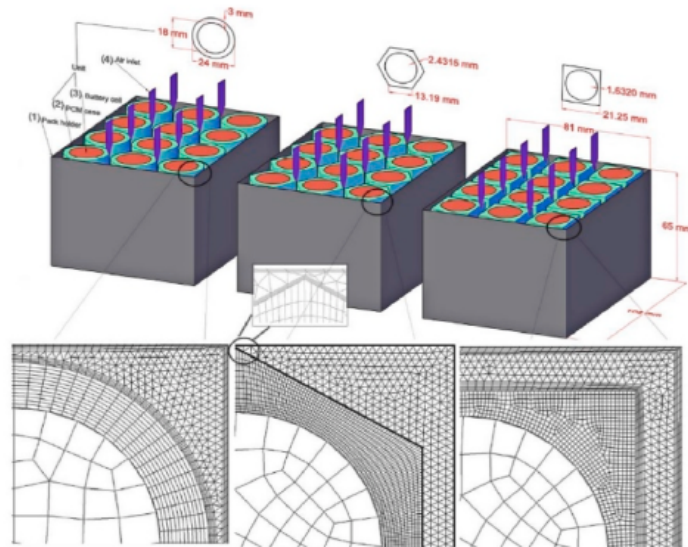
FIGURE 2.6: The schematic and experimental graphics show a PCM-based Battery Thermal Management System (BTMS) with integrated triangular, rectangular, and circular fins [45].
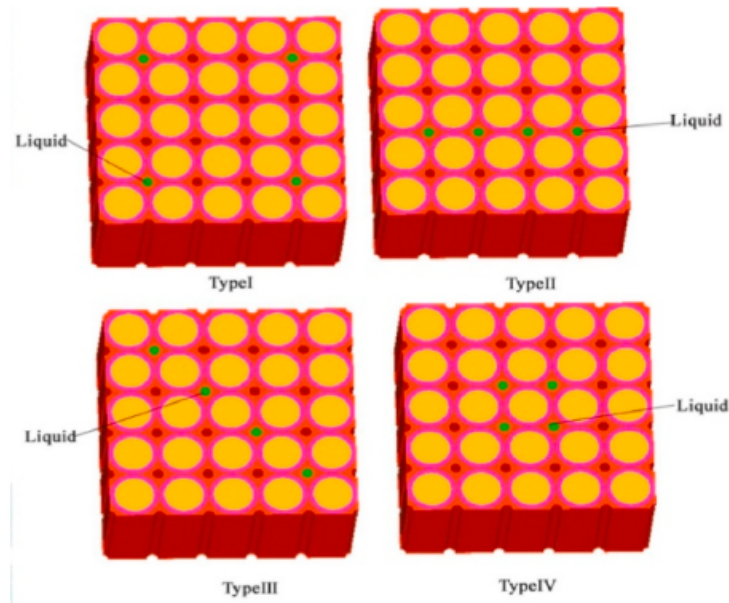
FIGURE 2.7: PCM liquid hybrid systems [47].

Wu et al. [48] proposed a BTMS that combines PCM with a heat pipe. In this arrangement, the evaporator section of the L-shaped heat pipe was sandwiched between PCM plates, while the condenser section extended outside the battery pack (Fig. 8c).

The incorporation of the heat pipe in the PCM-based BTMS reduced the maximum battery temperature from 53.2 to 50.9°C. They experimented further by combining the condenser part with forced air at velocities of 1, 2, and 3 m/s, lowering the maximum battery temperature to 50.9-47.2°C. Despite these enhancements, the hybrid BTMS did not significantly increase temperature difference when compared to the PCM-based BTMS.
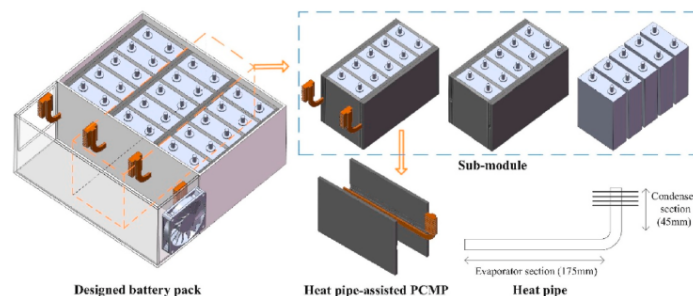
FIGURE 2.8: The graphic depicts three different configurations of air-based hybrid Battery Thermal Management Systems (BTMS) using circular, hexagonal, and rectangular CELL-PCM unit forms [48].

Chen et al. [49] examined maintaining the temperature of Li-ion batteries during a 3 C discharge rate; the study used paraffin/EG paired with liquid cooling. Four distinct liquid cooling arrangements were investigated.

In type 1, liquid circulated through four corner channels, but in types 2 and 3, it flowed through four vertical and diagonal channels. Type 4 involved a liquid travelling via four central channels. Both layout types 1 and 4 were equally effective at reducing temperature and ensuring consistency. Variations in liquid velocity ranged from 0.2 to 0.14 m/s. Beyond a velocity of 0.8 m/s, there was no substantial drop in battery temperature.

Shojaeefard et al. [50] conducted a study to investigate BTMS using six different fin types combined with PCM cooling. The results indicated that the horizontal fins had the optimum cell temperature control as compared to other fin arrangements and types. The results also indicated that the BTMS temperatures are affected by changing the fin alignment. Youssef et al. [51] conducted a unique design optimization to study the thermal performance of large Li-Ion batteries undergoing high discharge rates and cyclic loading.

Results showed that out of all cooling methods, PCM combined with jute gave the lowest temperature of 35.09 °C. At very high discharge rates the PCM combined with the jute cooling system gave the highest temperature of 36.29 °C. This study did not account for the life cycle assessment of PCM-Jute degradation. Huang et al. [52] numerically and experimentally studied BTMS using PCM 18650 Li-Ion batteries connected in parallel.

The BTMS is analyzed based on the heating rate model developed from the internal resistance of the cell. Results showed that the battery temperatures are lowered when the thermal conductivity of the PCM changes. However, at very high thermal conductivities, between 5-15 W/m-K, the temperature change is not significant.

The lowest temperature of the cells achieved in this study was $44.5°C$. El Idi et al. [53] investigated a BTMS on a fundamental level by using a single Li-Ion cell combined with metal foam added to the PCM. Both numerical and experimental

analyses were performed to investigate the ability of PCM and CPCM to absorb the heat produced by the cell. Specifically for the numerical analysis a novel battery test bench was also developed.
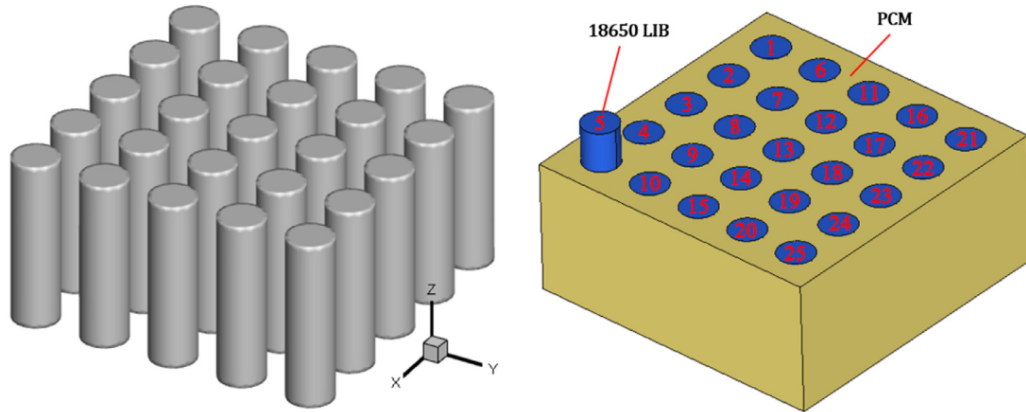
FIGURE 2.9: Physical representation of a LIB pack with 25 18650 cell units before and after packing with PCM [52].

The results revealed that adding aluminum foam to the cell allows for more efficient thermal control. The optimization investigation revealed that the thickness of PCM has very significant effects on the BTMS. It was also discovered that adding an extra volume of PCM has little effect on the cell surface temperature. Investigated PCM-based BTMS where the PCM is present around the boundary of the battery pack. Capric acid is used as PCM in this BTMS. PCM thickness optimization was also done with PCM thickness ranging from 3-7 mm. The effect of ambient temperatures on the BTMS was also studied considering two ambient temperatures $21°C$ and $50°C$. Furthermore, the effect of simple paraffin is compared to the Capric acid. The results showed that the PCM thickness of 3mm gave the optimum and lowest cell temperature of $32°C$. The battery can likewise be emulated with a solid cylinder of fixed voltage supply. For instance, Duan and Naterer [54] conducted a study on a heater enclosed by PCM and performed a comparison using several voltage supplies: 1.5 V, 4.5 V, 7.5 V, and 12 V. The findings demonstrated a decrease in the maximum temperature and unevenness while utilising Phase Change Material (PCM). Hemery et al. [55] studied the effects of increased internal resistance with age and thermal runaway when a cell short circuits in lithium-ion batteries. In this study, for safety considerations, a

combination of electrical heaters enclosed in a casing was used instead of actual cells along with forced air convection as a cooling medium.
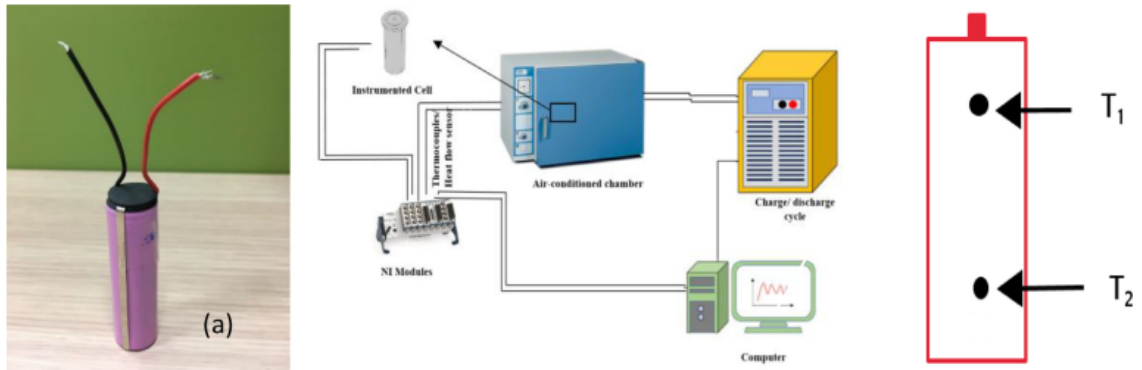
FIGURE 2.10: The experimental testbed includes a sample battery cell, a synoptic view of the testbed, and thermocouple locations [53].

The cell surface temperature under failure was maintained at $60°C$ in the PCM-enhanced BTMS. In the case of forced convection by air, the cell temperature exceeded $60°C$. Also, the volume percentage of PCM-enhanced BTMS was reduced from 79.7% [56] to 25% in comparison with the previous studies.
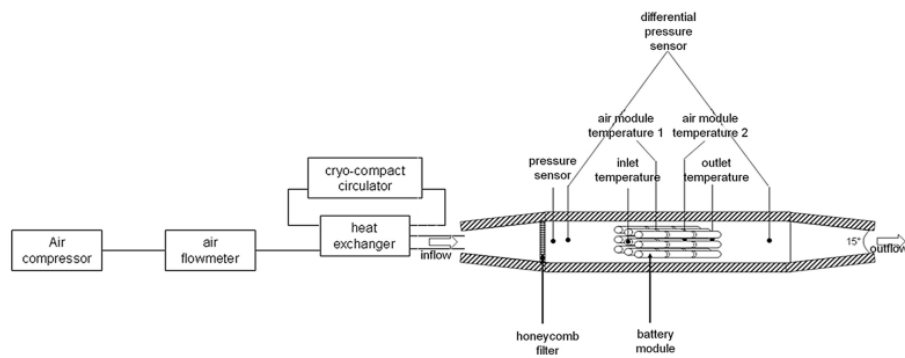
FIGURE 2.11: Schematic of the apparatus [55].

2.1 Current Methodology

The present investigation is centered on using experimental as well as numerical methods to improve the energy and thermal performance of BTMS. To the best of the author's knowledge, a PCM-fins combined BTMS using a battery test bench and steady-state Discharge rates (heat generation rates) has not been studied.

Also, the effects of tilting angle(Taper fins) as compared to the rectangular fins with a constant effective fin surface have not been analyzed before. A novel battery test bench is developed to analyze Lithium-Ion cells made from aluminum combined with specialized ceramic heaters forming a battery pack with different heat generation rates. The study also focuses on the comparison of convective and diffusive heat transfers for different fins cases including an unfinned case as well as Rectangular fins, Taper fins, and Circular fins. The performance would be enhanced with passive cooling by using Phase Change Material, Rubitherm GmbH RT-42. The need for numerical analysis along with concrete experimental results is due to the errors involved in experimentation. The number of sensors that could be used in a physical setup is limited which in some cases due to convection effects does not give correct thermal scoping. However, as a numerical solution deals with the area-weighted average of both the cell and PCM temperature gives accurate results to nullify the errors.

Chapter 3

Experimental Setup

3.1   Battery Thermal Management System Design

The BTMS design comprises three main components: the battery pack, with cells submerged in the PCM; a heat generation circuit connected to the cells; the Arduino Mega 2560, which sends temperature sensor data to a computer, as shown in Figure 3.1. The housing of the battery pack is made up of a 5mm acrylic sheet. A working flow model of these key components is shown in Figure 3.1. The battery pack contains four cells, which are equally spaced. The cells are the same dimensions as 18650 li-ion cells and are covered with aluminum material. A modified ceramic heater 10W3R3J is placed in a $10 \times 10 \times 65$ mm slot at the center of each cell to provide equal heat flux at each surface. A 2D representation of a cell with its dimensions is shown in Figure 3.2. The length, width, and height of the box, made out of acrylic, are 72 mm, 72 mm, and 85 mm, respectively. A fin thickness of 1 mm is constant for each case. The fin height is equal to the height H of the cells. The actual constructed LIB pack is shown in Figure 3.3. A brief schematic of the controller circuit and its working is shown in Figure 3.4. Thermocouples and LM-35 sensors provide temperature data for the PCM and cells, respectively. Further details of the circuit, heaters, and sensors are discussed in Section 3.1.2. The fin design was initiated from the rectangular fins from the

reference [57] and taper and circular fins are further modified keeping the surface area constant.
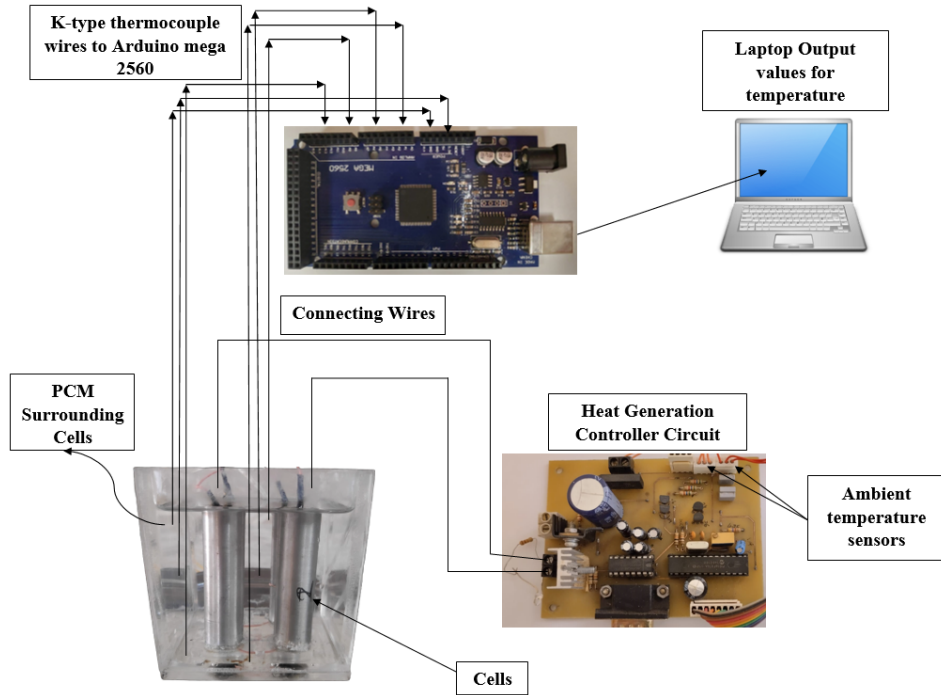
FIGURE 3.1: Schematic and working flow model of the proposed battery thermal management system.

3.1.1 Phase Change Material Selection Criteria

The Phase Change Material (PCM) selected is Rubitherm RT-42. The reason for choosing this specific PCM is that the author aims to test the BTMS under higher, as well as moderate ambient temperatures. keeping that in mind the PCM selected had a melting range of $38°C$ to $43°C$, which is suitable for testing under both temperature ranges. The selected PCM is chemically inert and stable with long cyclic life. RT-42 is an organic PCM with very high heat capacity(latent) which is advantageous for thermal energy storage and thermal enhancement applications.

3.1.2 Controller Circuit and Heat Generation Rates

The controller circuit was made up of a combination of micro controllers to produce smooth pulse wave modulation (PWM) with the ability to vary the heating
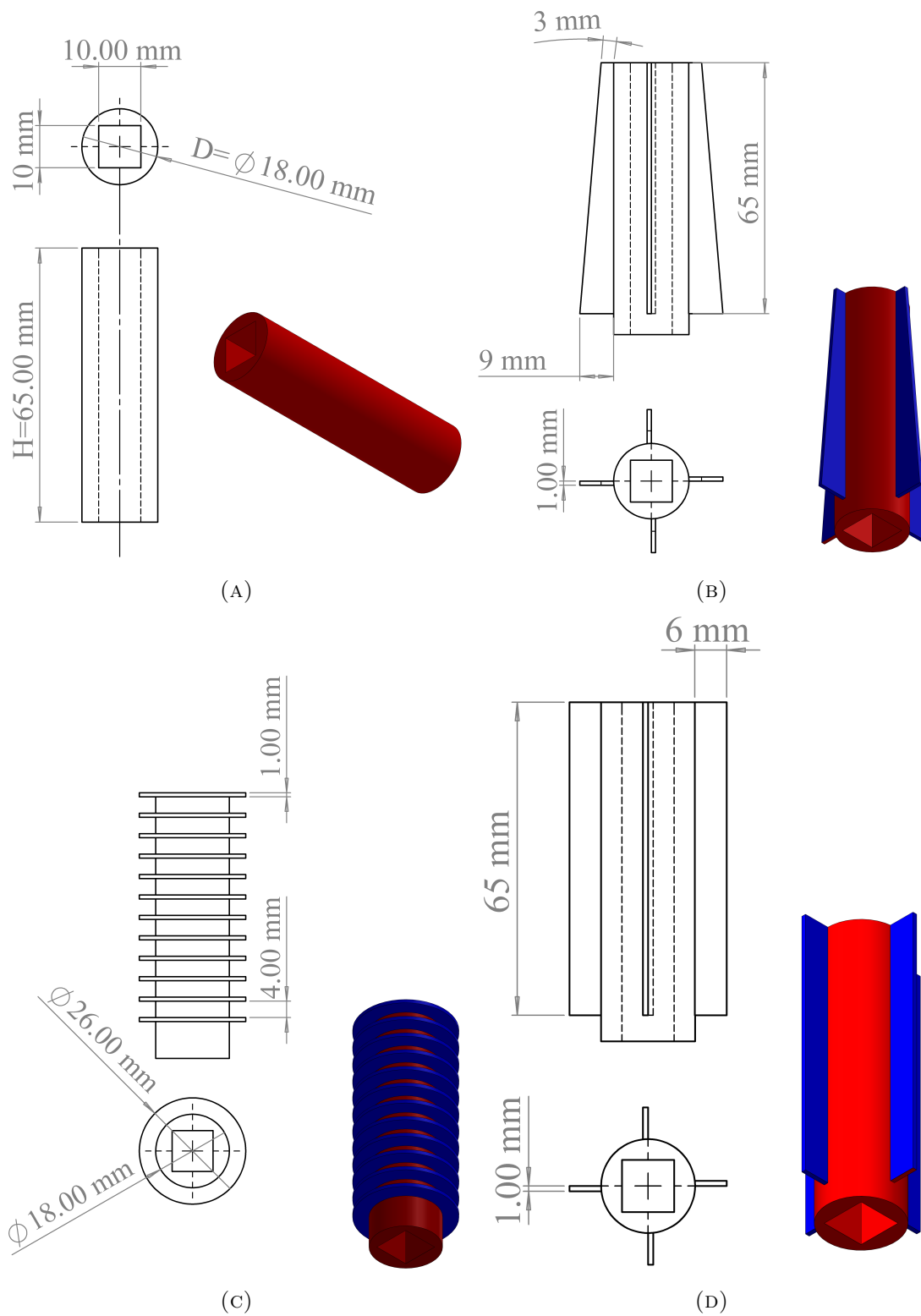
FIGURE 3.2: Detailed dimensions of the used fins: (**A**) the unfinned case; (**B**) taper fins; (**C**); circular fins; (**D**) rectangular fins [57].
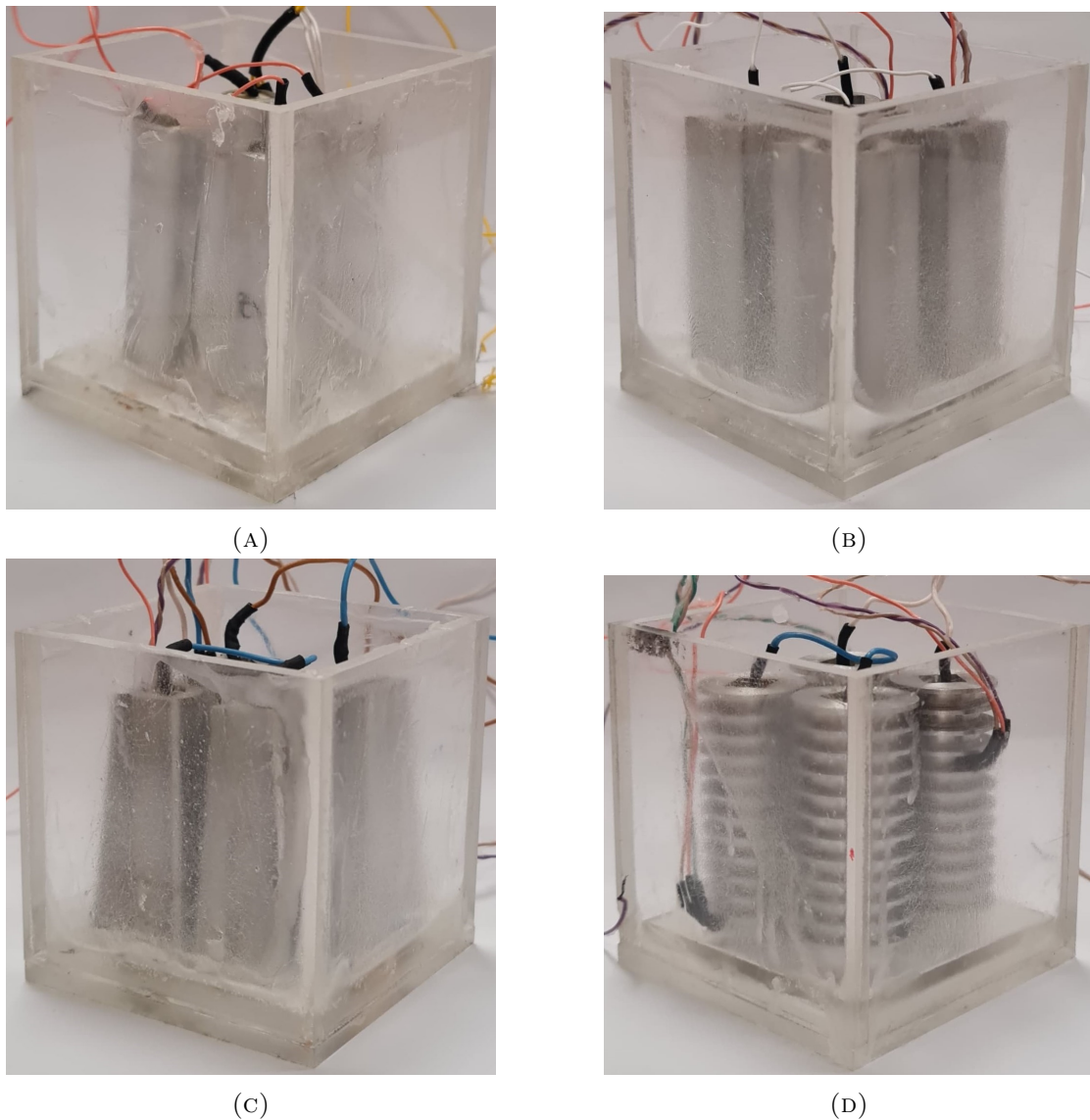
FIGURE 3.3: Illustration of the actual manufactured and assembled BTMS with all electrical connections to heaters: (**A**) the unfinned case; (**B**) rectangular fins; (**C**) taper fins; (**D**) circular fins.
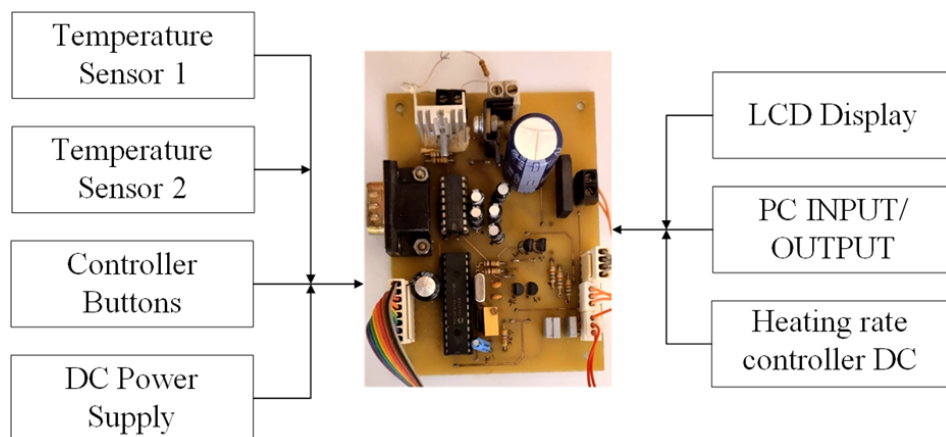
FIGURE 3.4: Schematic to explain the working of the battery simulator, as well as a visualization of the actual circuit.

rate for the ceramic heaters from 0.05 W to 6 Watts in the complete circuit, accommodating all losses. The ceramic heaters used in this study and their assembly in the unfinned case are shown in Figure 3.5.

FIGURE 3.5: (**A**) Ceramic heater used for volumetric heat generation; (**B**) CAD illustration of the assembly of a ceramic heater fixed in an unfinned cell.

The heat generation rates used, as quoted by Choudhari et al. [57], are shown in Figure 3.6. The heating rate for 1C was 0.2 W, 2 C was 0.7 W, and 3 C was 1.5 W per cell. So, for the 4-cell configuration, the circuit needed a heating rate of 4 times the rating. The steady-state heating rate applied for 1C was 0.8W, 2C was 2.80 W, and 3C was 6 W. The cell surface temperature was measured using an LM-35 temperature sensor with a tolerance of ±0.25 °C.

The cell surface temperature was measured at two locations with offsets from the top and bottom of the cells. Additionally, six K-type thermocouples with an accuracy of ±1.5 °C were used to measure the temperature of the PCM. Arduino Mega 2560 and Arduino Uno were coded and used for the temperature measurements. For the constant ambient temperature measurements, the control circuit was maintained at 27°C.

The thermocouple locations were set to scope the height of the box, as well as the length and width, to ensure the accuracy of PCM temperature measurements. The cycle time used to observe temperature evolution was kept fixed at 60 min

for all cases. The T_{ref} for each cell was 23.18°C and the T_{ref} for the PCM was 26.29°C.

3.1.2.1 Controller Circuit Validation and Response Time

The controller circuit was validated using the heat generation rate of circuit and Choudhari et al. [57]. The validation is shown in Figure 3.6.
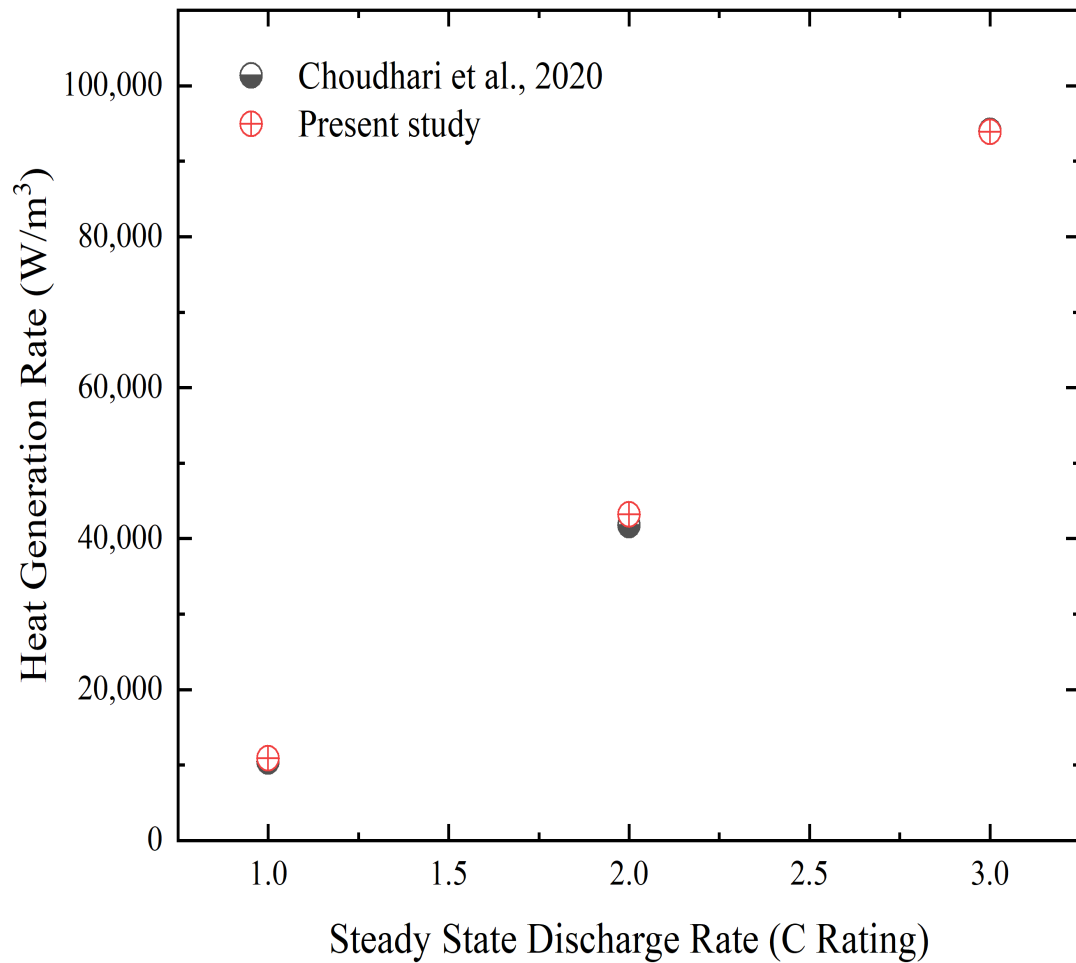
FIGURE 3.6: Controller circuit validation with Choudhari et al. [57].

The validation shows the heat generation rates produced by Choudhari et al. [57] and the completely overlapped reproduced heat generation rates in the current study.

Moreover, the temporal response time to reach these respective heat generation rates and their corresponding powers are also shown in Figure 3.7.
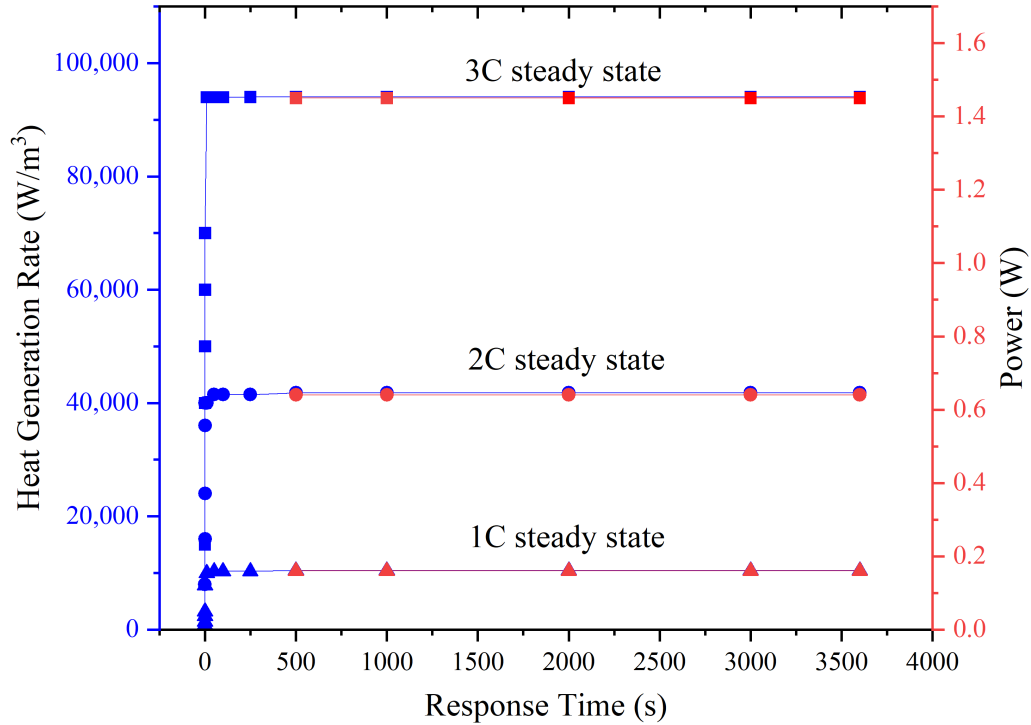
FIGURE 3.7: Temporal response times for heat generation in the controller circuit, as well the corresponding power.

The temporal response time for the controller circuit validates the steady state condition for the heat generation rates and power. This temporal response time and the steady state behavior helps in simplification of the cell discharge rates and the time dependency of C ratings for the 18650 Li-Ion cell can be disregarded.

3.1.3 Sensor Placement

The precise positioning of sensors was a crucial step in the construction of the Battery Thermal Management System (BTMS). The utilisation of six K-Type thermocouples was important in quantifying the behaviour of Phase Change Material (PCM).

The placement of these thermocouples was strategically determined based on Figure 3.8. Due to the symmetrical construction of the battery pack, sensors were placed at three distinct depths: completely submerged, slightly submerged, and near the upper surface of the PCM. The entire technique allowed for precise temperature monitoring and assessment of convection effects within the PCM.

(A)   (B)
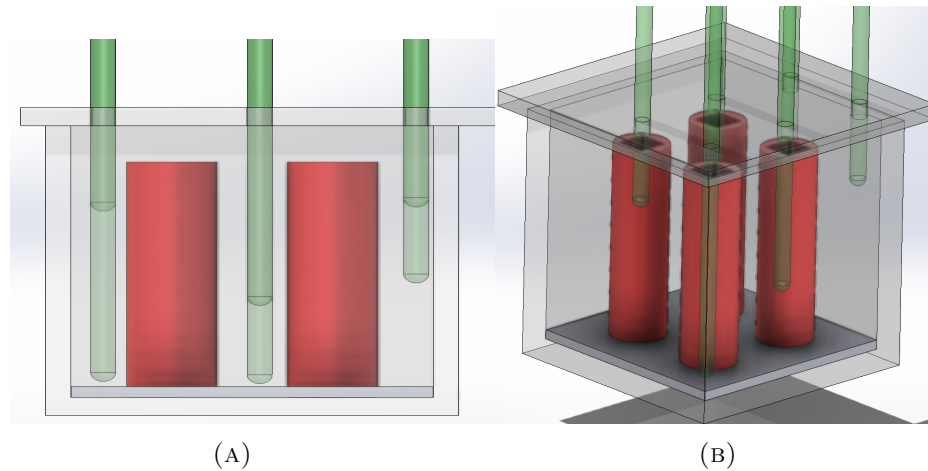
FIGURE 3.8: PCM sensors placement in the LIB pack in (A) Side view (B) Isometric view.

The positioning of the two temperature sensors within the cells adhered to the arrangement illustrated in Figure 3.9. The grey bodies are an illustration of the cell temperature sensor LM-35. Both the top and bottom sensors record similar readings during the conduction phase of the Phase Change Material (PCM) and the cell.

However, as soon as the melting process starts, it would became clear that there was a noticeable difference in temperature between the upper and lower parts of the cell. This discrepancy is crucial for examining the dynamics of cell temperature and comprehending the thermal behaviour throughout the phase of melting.
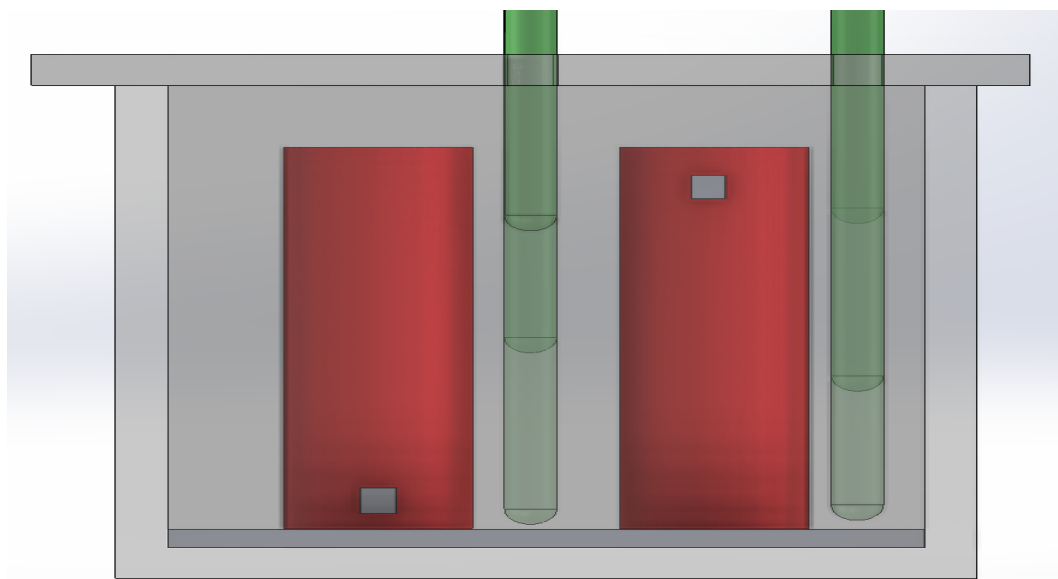
FIGURE 3.9: Cell temperature sensor placement at the top of one cell and the bottom of another cell.

Chapter 4

Numerical Methodology

4.1   Domain Discretization and Mesh

A two dimensional simplified model along the diagonal section was defined from the 3D CAD model of the LIB pack The 3D CAD model of the LIB pack is shown in Figure 4.1.
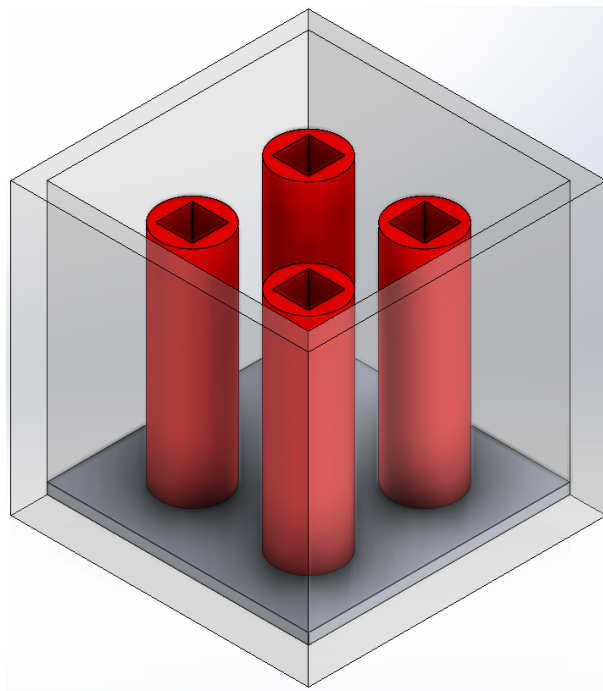
FIGURE 4.1: 3D CAD of the unfinned case.

The section from the diagonal direction was obtained by rigorous numerical optimization considering different section views which then led to the diagonal direction being the optimum case.

The section view from the CAD model obtained is shown in Figure 4.2. This CAD was then created in ANSYS for the numerical analysis which is shown in Figure 4.3
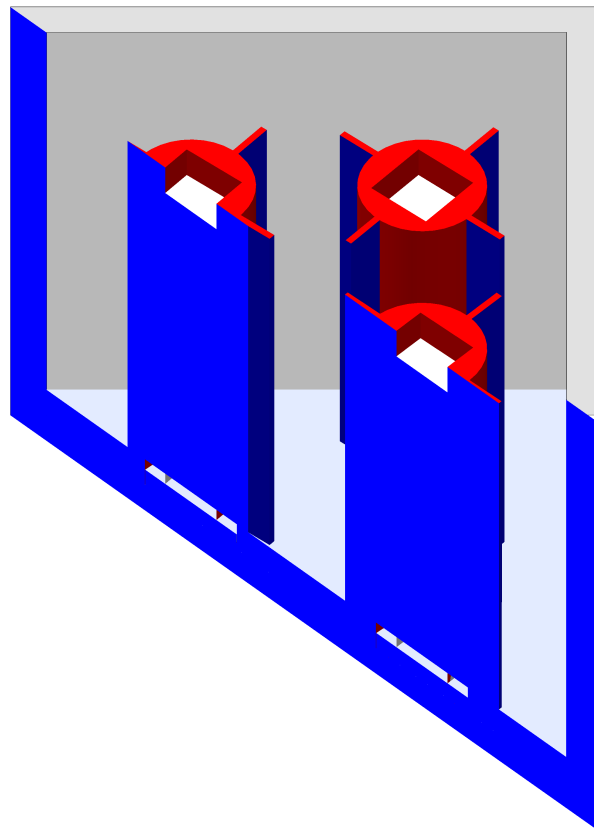
FIGURE 4.2: Section view from the 3D CAD in the diagonal direction.
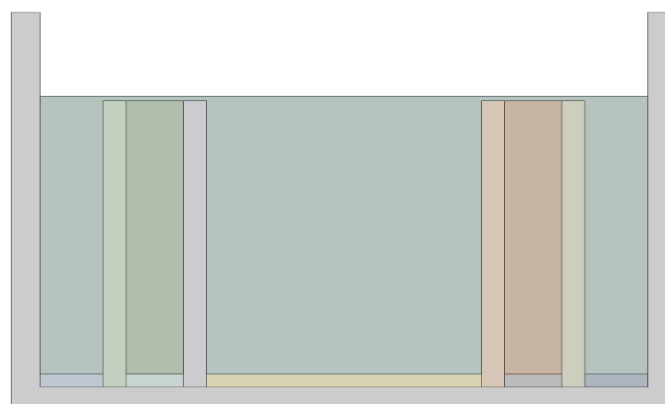
FIGURE 4.3: Diagonal 2D domain generated in ANSYS workbench.

4.2   Numerical Problem Formulation

A buoyant two-phase (solidification/melting) laminar flow was simulated using ANSYS Fluent 2021R2. In order to perform numerical simulations, several assumptions were made and the system was simplified. The liquid phase of the PCM was defined as an in-compressible, Newtonian, homogeneous, and isotropic media and the radiation heat transfer was deemed insignificant compared to natural convection heat transfer.

The buoyant force caused by temperature-dependent density fluctuations during PCM melting was modeled using the Boussinesq approximation. The volume expansions of the PCM were likewise omitted when using the Boussinesq approximation and natural convection was assumed to be laminar. For a proper comparison of results, two of the cell cases were chosen based on the experiments performed in the current study: the unfinned (base case) and the best-performing rectangular fin case.

4.2.1   Governing Equations

PCM melting includes a complicated two-phase flow simulation with strong natural convection effects. As a result, the enthalpy porosity approach of Voller and Prakash [58] was used to simulate the phase transition process using a single set of governing equations. The equations for continuity, momentum, and energy are shown in Equations (4.1)–(4.3), respectively.

$$\frac{\partial \rho}{\partial t} + \frac{\partial (\rho u_i)}{\partial x_i} = 0 \tag{4.1}$$

$$\frac{\partial (\rho u_i)}{\partial t} + \frac{\partial (\rho u_i u_j)}{\partial x_j} = -\frac{\partial p}{\partial x_i} + \mu \frac{\partial^2 u_i}{\partial x_j \partial x_j} + F_{B_i} + F_{Mi} \tag{4.2}$$

$$\frac{\partial (\rho h)}{\partial t} + \frac{\partial (\rho u_i h)}{\partial x_i} = \frac{\partial}{\partial x_i} \left(\lambda \frac{\partial T}{\partial x_i} \right) \tag{4.3}$$

where g, u, ρ, μ, and p are the gravitational acceleration, velocity density, viscosity, and pressure, respectively. Natural convection is induced during PCM

melting due to temperature-dependent density differential and gravitational influences. The momentum equation's buoyancy source term F_{Bi} was solved using the Boussinesq approximation: $F_{B_i} = \beta \rho (T - T_l) g$. In the energy equation, λ, h, and T are the thermal conductivity, enthalpy, and temperature, respectively.

4.2.2 Enthalpy Variations

Depending on the phase of the material, PCM enthalpy variations can be divided into three primary stages: (i) fully solid PCM; (ii) partially liquid and solid PCM; and (iii) fully liquid PCM. Equation (4.4) represents the phase segregation-based mathematical expressions for these enthalpies.

$$
h = \begin{cases}
\int_{T_R}^{T} C_{p_s} \, dT, & \text{if } T < T_s \\[2mm]
\int_{T_R}^{T_s} C_{p_s} \, dT + \Delta H, & \text{if } T_s \leq T < T_l \\[2mm]
\int_{T_R}^{T_s} C_{p_s} \, dT + \Delta H + \int_{T_l}^{T} C_{p_l} \, dT, & \text{if } T \geq T_l
\end{cases}
\tag{4.4}
$$

where T_R is the reference temperature, which had the value of 27 °C in this study.

4.2.3 Melting Fraction

The latent heat content is denoted by ΔH, while the specific heat for liquid and solid PCM is denoted by C_{pl} and C_{ps}, respectively. The PCM melt fraction (δ) is given in Equation (4.5).

$$
\delta = \frac{\Delta H}{L_{\text{PCM}}} = \begin{cases}
0, & \text{if } T < T_s \\[2mm]
\dfrac{T - T_s}{T_l - T_s}, & \text{if } T_s < T < T_l \\[2mm]
1, & \text{if } T > T_l
\end{cases}
\tag{4.5}
$$

Similar to the enthalpy variations, the melting fraction has three stages: (i) when temporal temperature is below the solidus temperature of PCM, the melting fraction is 0; (ii) when temporal temperature is above the liquidus temperature, the

melting fraction is 1; (iii) when the temporal temperature is between the liquidus and solidus temperatures, the melt fraction is calculated using the ratio of the difference between the liquidus and solidus temperatures to the difference between the temporal and solidus temperatures.

4.2.4 Momentum Source Term

The momentum variation in liquid PCM induced by natural convection is described by the source term F_{Mi} in Equation (4.2). Additionally, Equation (4.6) represents the damping source term, which is characterized by Darcy's law according to the model proposed by Olabi et al. [59].

$$F_{Mi} = \frac{A_{\text{Mushy}}(1 - \delta)^2}{\delta^3 + \xi} u_i \tag{4.6}$$

where A_{Mushy} serves as the mushy zone constant responsible for velocity damping. Values of A_{Mushy} generally range from 10^4 to 10^7. The higher the value of A_{Mushy}, the slower the melting. The A_{Mushy} value chosen for this case was 10^5.

4.3 Discretization Schemes and Solutions

The governing equation's diffusive part was resolved using a second-order central differencing scheme and the momentum term was solved using the pressure staggering option (PRESTO) scheme. In the energy and momentum equations, the convection terms were resolved using a third-order monotone upstream-centered scheme for conservation laws ($MUSCL$). Temporal discretization was achieved using a second-order implicit scheme, which is very stable.

To obtain accurate results, the convergence criteria were set to 10^{-6}. For the pressure-velocity coupling, the semi-implicit method for pressure-linked equations (SIMPLE) was used. In the SIMPLE procedure, the relationship between pressure and velocity corrections is employed to solve for mass conservation and determine the pressure field. The face flux, denoted as J_f^*, is computed by solving the momentum equation with a guessed pressure field p^*.

4.4 Boundary Conditions, Initial Conditions, and Thermophysical Properties

The boundary and initial conditions used in the numerical analysis were as follows:

1. The control volume for the heaters was given a volume condition as the heat generation rate (W/m³), according to Choudhari et al. [57], which was 94,023.8 (W/m³) for 3C, 41,788.37 (W/m³) for 2C, and 10447 (W/m³) for 1C;

2. The walls were exposed to the environment as the system was not kept adiabatic and had a natural convection coefficient of 2.5 W/m².K;

3. The mushy zone constant was kept at the default level and solidification and melting were used to simulate the phase change process;

4. All thermophysical properties for both the numerical and experimental setups are shown in Table 4.1;

5. The solution was initialized and patched with 23.18 °C for the cells and 26.29 °C for the PCM, fins, and base plate temperatures, while the housing, which is exposed to the environment, was kept at 27 °C. The reason for these selected temperatures was to maintain uniform reference temperatures for both the experimental and numerical analyses.

TABLE 4.1: Thermophysical properties used in the experimental and numerical models.

Property	RT-42	Aluminum	Acrylic	Ceramic Heaters
Solidus Temperature (°C)	38	-	-	-
Liquidus Temperature (°C)	43	-	-	-
Heat Storage Capacity (J/kg)	165,000	-	-	-
Specific Heat Capacity (kJ/kg.K)	2	871	1300	850
Solid Density (kg/m^3)	880	2719	1215	2630
Liquid Density (kg/m^3)	760	-	-	-
Thermal Conductivity (W/m.K)	0.2	152	0.17	12
Thermal Exp. Coefficient (K^{-1})	0.0006	-	-	-

4.5 Timestep and Mesh Independence Study

To eliminate the effects of mesh and timestep on the solution, a mesh and timestep independence study was conducted. Three different grid sizes were created: 10000, 20033, and 36668 elements. Also, for timestep independence, 0.5 s, 0.25 s, and 0.125 s were investigated on a grid size of 20033 elements. No significant deviations were observed during either study. So, a timestep size of 0.5 s and a grid size of 20033

elements were chosen. Figure 4.4 shows the time–temperature curve for each of the element sizes and timesteps.
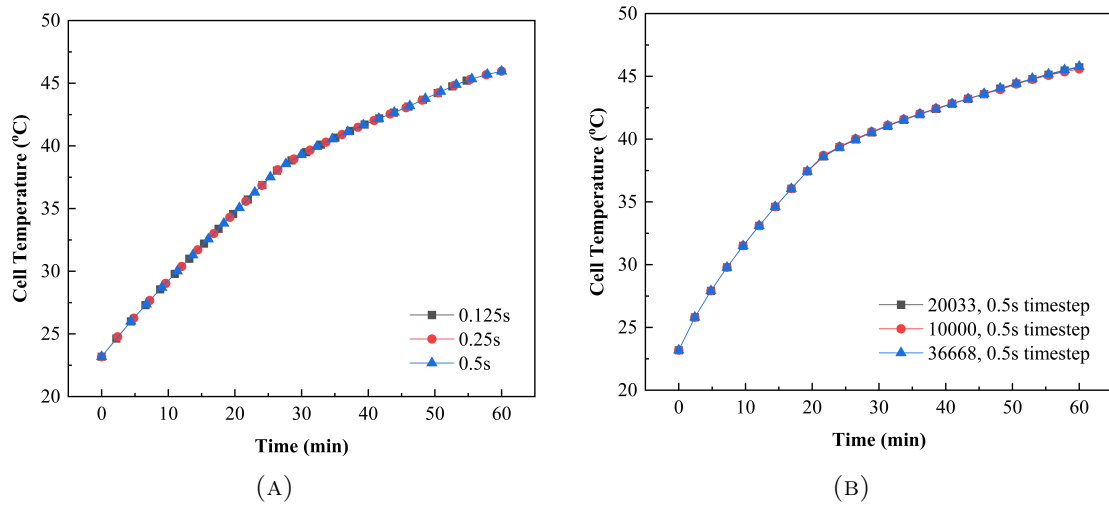
FIGURE 4.4: (**A**) Mesh independence; (**B**) timestep independence.

The mesh selected after the mesh independence study consisting of 20033 elements is shown in Figure 4.5
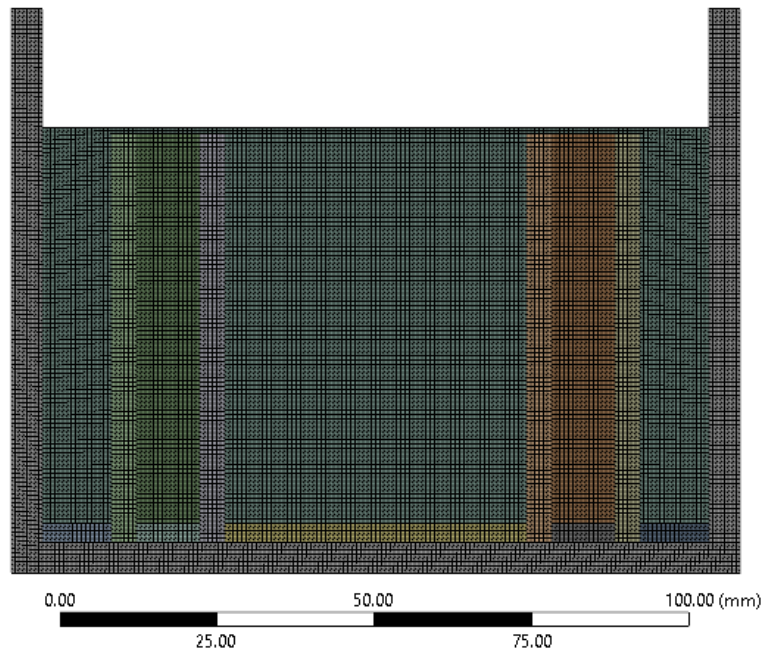
FIGURE 4.5: Orthogonal mesh with 20033 elements constructed in ANSYS meshing for the numerical analysis.

Chapter 5

Results and Discussion

5.1 Experimental Results

The performance of each case was evaluated based on its geometry. The main parameter under study was cell temperature. The base case, which was the unfinned case, was also evaluated without the PCM, which helped to create the baseline reference temperatures to compare the results to after the addition of the PCM and different fin structures

5.1.1 Temporal Temperature Variation at 1C Discharge Rate

At 1C discharge rate the cell temperatures for all the cases are shown in Figure 5.1. Initially, the cell temperature for the unfinned case rises which is then controlled by the PCM by conduction. Due to low heat generation rate at 1C discharge rate, all the cases remain in the conduction region with the PCM and below the optimum temperature 40 °C. However, the unfinned case attains the highest temperature amongst other finned cases showing the worst thermal performance. The rectangular fins case supersedes all the other finned and unfinned cases and shows the lowest temperatures. The Figure 5.1 shows another key comparison of the effectiveness of introduction of PCM in the Battery pack by comparing the

unfinned case in PCM with unfinned case in the ambient environment (without PCM).

FIGURE 5.1: Temporal temperature variation at 1C discharge rate for all finned and unfinned cases in PCM and in natural convection.

5.1.2 Temporal Temperature Variation at 2C Discharge Rate

At 2C discharge rate the cell temperature variation with time is shown in figure 5.2. This intermediate discharge rate has a corresponding heat generation rate of 41788.37 W/m^3 which in the case of unfinned ambient cell, crosses the optimum temperature after 20 mins out of the 60 mins cycle time.

However, when the cells are placed in PCM for each of the finned and unfinned case, neither cases finned or unfinned cross the optimum temperature. Amongst the cell cases placed in PCM, the unfinned case following the trends of 1C discharge rate has the worst performance. The rectangular fins case shows the most effective performance lying close to the circular fins as shown in Figure 5.2.

FIGURE 5.2: Temporal temperature variation at 2C discharge rate for all finned and unfinned cases in PCM and in natural convection.

5.1.3 Temporal Temperature Variation at 3C Discharge Rate

The temporal temperature variation at 3C discharge rate is shown in Figure 5.3. This is the highest discharge rate with corresponding heat generation rate of 94023.8 W/m³. The cells reach the highest temperatures at this discharge rate and have a rapid slope of temperature increase as it can be seen for the unfinned ambient case which crosses the optimum temperature at around 5 mins. The induction of PCM into the LIB pack enhances the thermal performance of the cells and it can be observed that the slope of the temperature increase is controlled in each case by the melting of the PCM. During both conduction region and melting region the unfinned case has the highest temperature and crosses the optimum temperature at around 30 minutes. However, the optimum case rectangular fins reaches that temperature at round 45 minutes. Each of the finned and unfinned cases are above the optimum temperature at the end time of 60 mins with the lowest temperatures achieved by the rectangular fins.
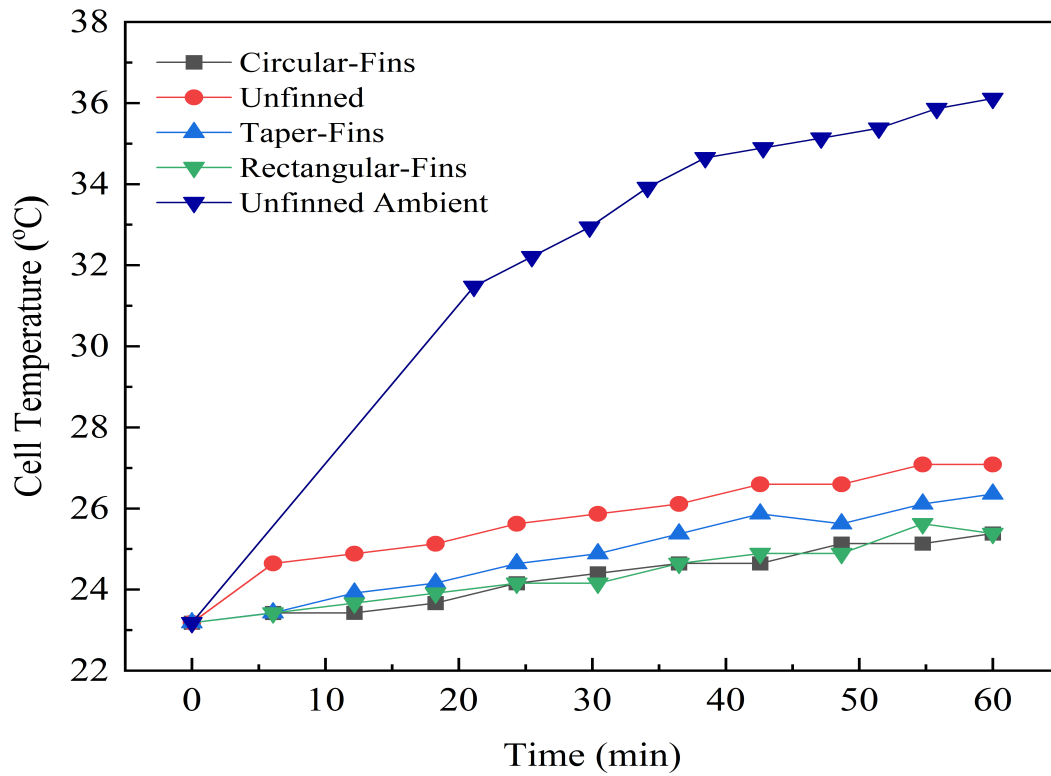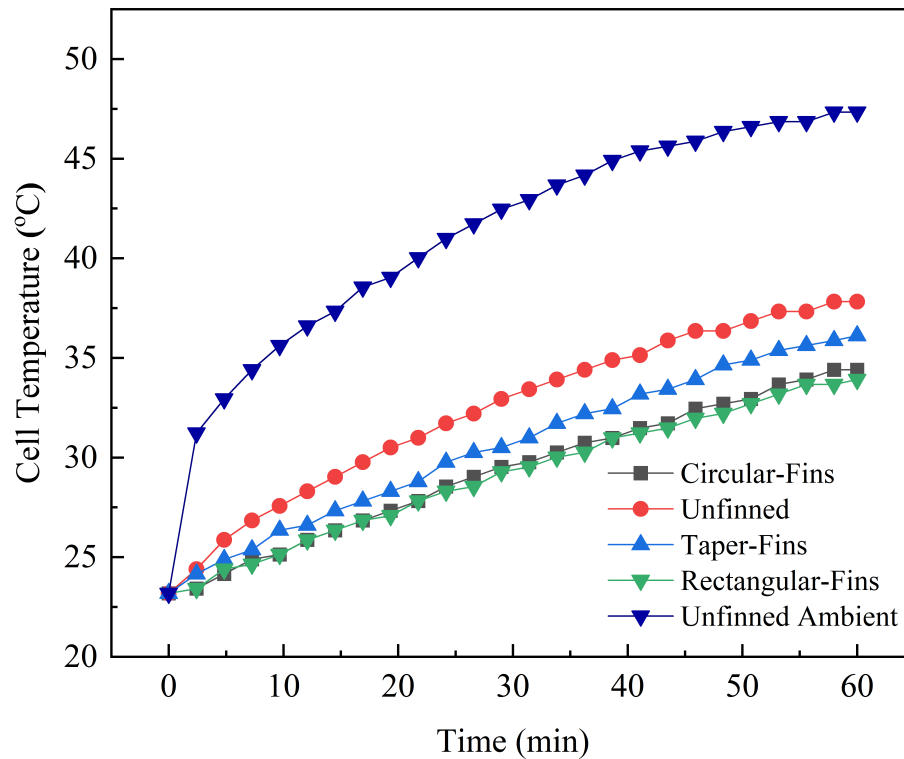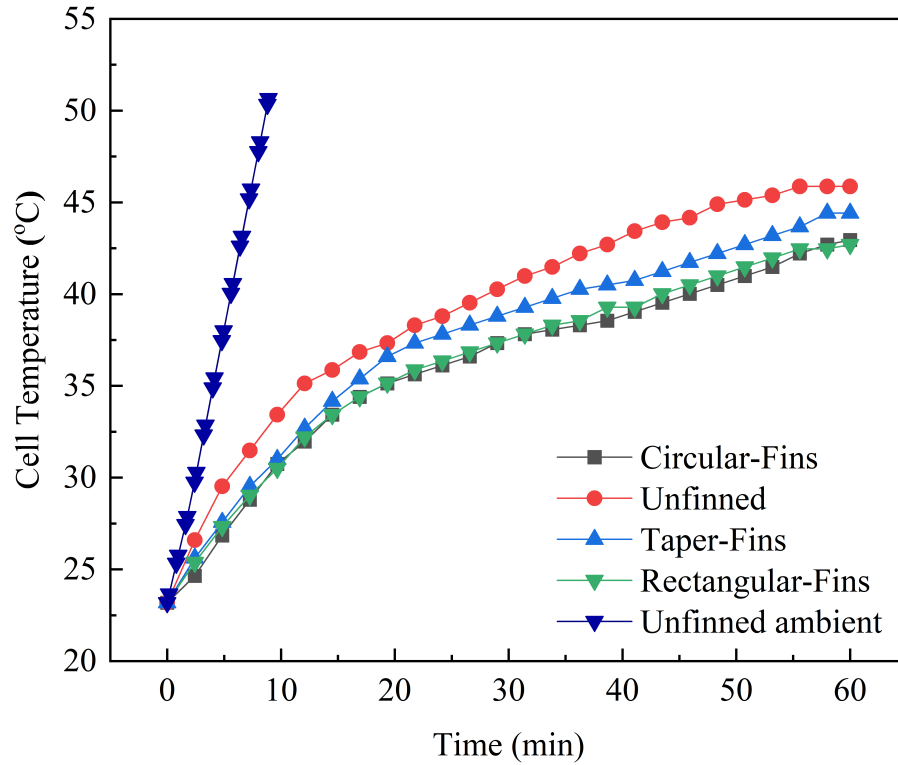
FIGURE 5.3: Temporal temperature variation at 3C discharge rate for all finned
and unfinned cases in PCM and in natural convection.

To summarize, The temperature variation in the 3C discharge rate is shown in
Figure 5.3, in which the unfinned case had the maximum temperature due to
heat accumulation after the melting front completely traveled away from the cell
surface. The maximum temperature achieved for the unfinned case was 45.87 °C
at 60 min. That is 5.87 °C beyond the maximum temperature for 18650 li-ion
cells. The taper and circular fin cases had maximum temperatures of 44.4 °C and
42.9 °C, respectively.

However, the rectangular fin case was the best-performing case in all of the exper-
iments performed, having a maximum temperature of 42.7 °C at 60 min. The per-
centage decrease in temperature achieved for the 3C discharge rate with the rectan-
gular fins was 6.91%. Although the temperature at 60 min was above the optimum
temperature, it can be seen that a significant increase in operation time to achieve
the maximum optimal temperature. For instance, an unfinned case achieves 40 °C
at 28.08 min. However, the rectangular fins case achieved a temperature of 40 °C
at 43.17 min, which represented approximately 15 min more operation time below

the maximum temperature.

The reason for the increase in temperatures above the optimal cell temperature was because of the 0.2 W/m.K thermal conductivity of the phase change material, which created a thermal barrier with its high storage energy when the melting front was away from the cell surface, as well as the fin surfaces.

Similarly, for the 2C discharge rate, the best-performing case was the rectangular fin case, with a maximum temperature of 33.915 °C. The unfinned case had the highest temperature of 37.82 °C, which showed that the rectangular fins had a very significant effect on the temperatures of the cells. All of the different geometries stayed below 40 °C for the 2C and 1C cases as the conduction region of the PCM was very effective at limiting the cell temperature.

Figure 5.1,5.2 and 5.2 shows the key difference and effectiveness of the addition of the PCM and fins in the lIB pack. As a comparison, it can be observed that the unfinned ambient 3C case achieved 40 °C at 5.6 min, whereas the unfinned case with the PCM achieved the same temperature at 28.42 min and the rectangular fin case with the PCM achieved it at 43.17 min, which were significant changes. For the unfinned ambient case at 1C, the temperature reached 36.11 °C at 60 min compared to the optimum rectangular fin case, which had a maximum temperature of 25.38 °C. So, a temperature improvement of 29.71% was observed for 1C. Similarly, for the 2C discharge rate, the maximum temperatures of the unfinned ambient and rectangular fin cases were 47.34 °C and 33.92 °C, respectively. A maximum temperature improvement of 28.35% was observed for the 2C discharge rate.

5.2 Thermal Performance of the BTMS

To evaluate thermal performance based on the temperature evolution during a fixed 60-min cycle for each discharge rate (heat generation rate), a performance enhancement factor Θ was defined, as shown in Equation (5.1).

$$\Theta(t) = \left| \frac{T_{\text{cell}}(t) - T_{\text{ref}}(t)}{T_{\text{initial}}(t) - T_{\text{ref}}(t)} \right| \tag{5.1}$$

where T_{cell} is the temperature at $t = 60$ min, T_{initial} is the initial temperature of the cell at $t = 0$ min, and T_{ref} is the reference temperature, which was the average ambient temperature kept constant at the time of each experiment and numerical simulation. Figure 5.4 depicts the thermal performance enhancement for the rectangular fin case, which was greater than all of the other cases (smaller bar heights represent better results) at the 3C and 2C discharge rates. However, the 1C case was only in the conduction region and the melting fraction remained zero throughout the time of the experiment and simulation, so the trends changed and the unfinned case performed better.

The thermal performance factors for each Discharge rate are shown in Table 5.1. The temperature ratio comparison shown in Figure 5.4 is based on the unfinned ambient case, which showed that the rectangular fin case at 3C tended to keep the temperature of the cells below the required level at $\theta = 4.18$. The circular fin case was at the borderline for the 3C discharge rate.
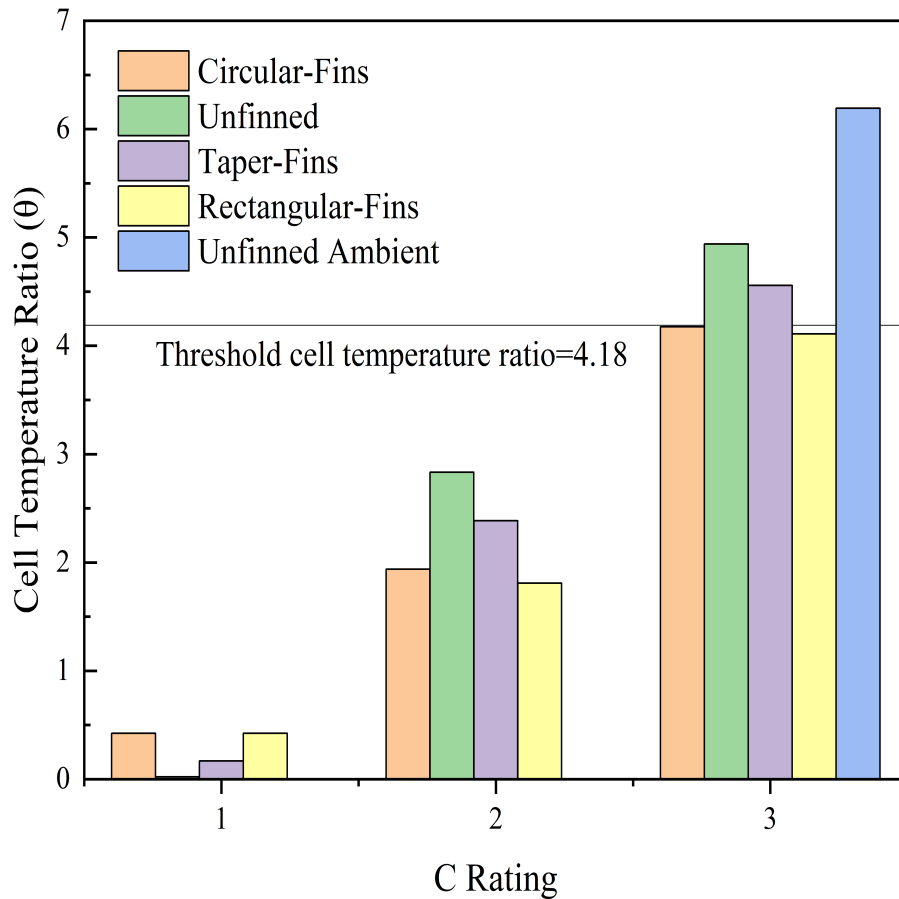

FIGURE 5.4: The thermal performance enhancement ratios at different discharge rates compared to the unfinned ambient case as a benchmark.

TABLE 5.1: Theta values at different discharge rates.

		θ		
Discharge Rate	Unfinned Case	Rectangular Fins	Taper Fins	Circular Fins
1C	0.023	0.42	0.17	0.42
2C	2.83	1.81	2.38	1.94
3C	4.94	4.11	4.56	4.18
3C Ambient	6.19			

5.3 Comparison of Numerical and Experimental Results

5.3.1 Numerical Validation

To verify the correctness of the numerical model, along with a comparison to the experimental results, the numerical model and methodology were also validated by reproducing the results and comparing them, as performed by [57]. Figure 5.5 shows the validation results with errors of less than 1%. This verified that the numerical model created was correct and would give accurate results.

5.3.2 Numerical vs Experimental Comparison of Cell Temperatures for Each Discharge Rate

The numerical model was validated using the experimental results from the unfinned and rectangular fin cases at each discharge rate to further verify the correctness of the experimental results. The numerical results comparison with the experimental results are discussed for each discharge rates in the sections below.

5.3.2.1 1C Discharge Rate

The comparison of the numerical results with the experimental data at 1C discharge rate at its corresponding heat generation rate for unfinned case is shown
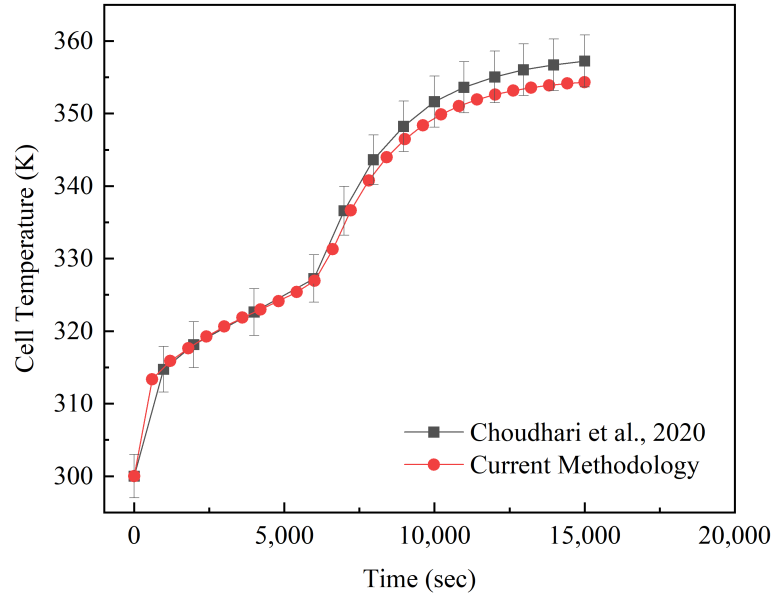
FIGURE 5.5: Numerical validation curve comparison to [57].

in Figure 5.6 and for the rectangular fins case is shown in Figure 5.7.The results showed a promising trend with an agreement to the experimental results comprising of error ranging from less than 1% to 5% over a 60 minutes cycle time. The error bars for unfinned case are plotted at 5 percent. The curve detaching from the experimental results is due to the LM-35 sensor fluctuations and the number of cell temperature sensor being less for the experimental results.

FIGURE 5.6: Comparison and validation of numerical prediction using experimental results for unfinned LIB pack at 1C discharge rate.
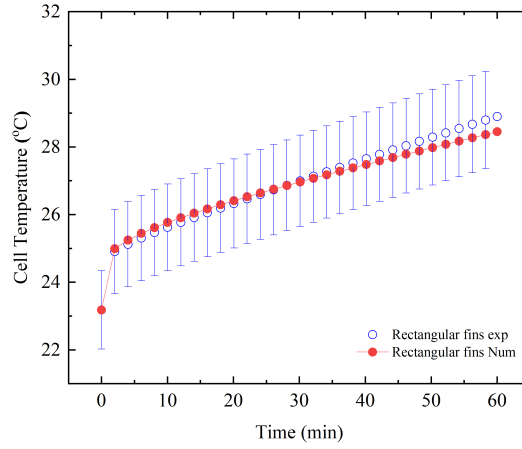
FIGURE 5.7: Comparison and validation of numerical prediction using experimental results for unfinned LIB pack at 1C discharge rate.

5.3.2.2   2C Discharge Rate

At 2C discharge rate the temporal comparison of experimental and numerical results shows that the cell temperatures tend to rise and detach the experimental results when time approaches 60 mins. This is due to the experimental data is limited to two sensors and the numerical results giving an area weighted average of the whole cell.

Overall, the results lie within error range of 5%. The comparison of results for unfinned is shown in Figure 5.8 and for the rectangular fins is shown in Figure 5.9
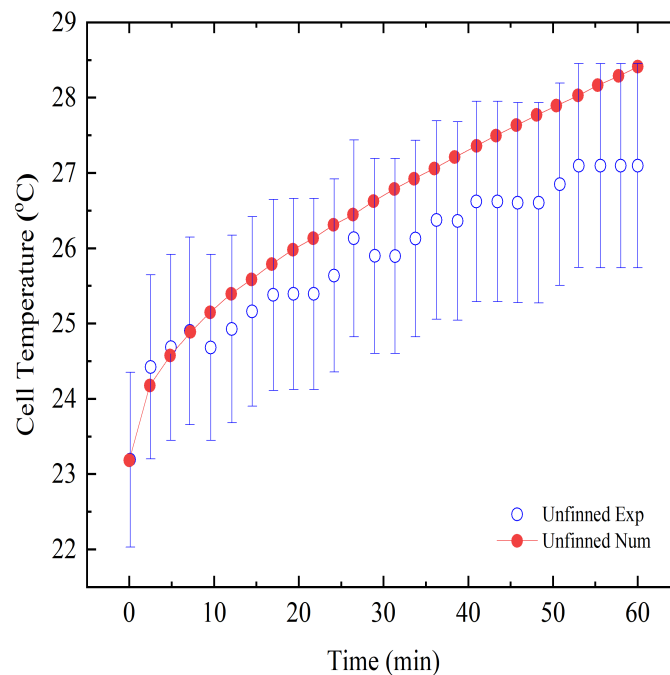

FIGURE 5.8: Comparison and validation of numerical prediction using experimental results for unfinned LIB pack at 2C discharge rate.

FIGURE 5.9: Comparison and validation of numerical prediction using experimental results for unfinned LIB pack at 2C discharge rate.

5.3.2.3   3C Discharge Rate

The numerical analysis comparison with experimental results at 3C discharge rate shows a promising trend to verify the correctness of the experimental results. For the unfinned case comparison due to weak convection effects the results lay within error range of less than 2%. The comparison is shown in Figure 5.10. Figure 5.11 illustrates a comparison between the average PCM temperatures obtained from numerical simulations and experimental data for the case of unfinned and rectangular fin cases. In the case of rectangular fins, the results agreement is strong for the initial 20 minutes, but beyond that point, a slight deviation emerges, approximately within a 5% range. This discrepancy is attributed to the onset of strong buoyancy effects during this period, leading to notable
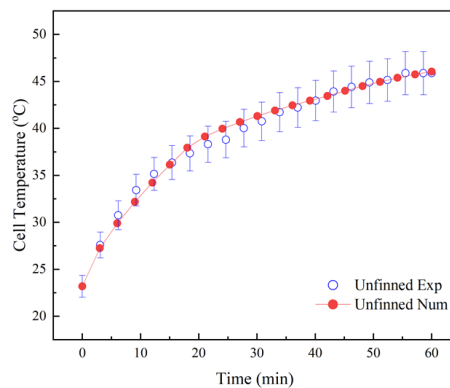
FIGURE 5.10: Comparison and validation of numerical prediction using experimental results for unfinned LIB pack at 3C discharge rate.

temperature variations in the axial direction of the PCM and consequently contributing to the observed mismatch in results. Therefore, rapid axial temperature variation and the limited number of sensors lead to such deviation. However, for unfinned cases, the results match quite well throughout the cycle since the buoyancy effects are not as strong as observed in the rectangular fin case.
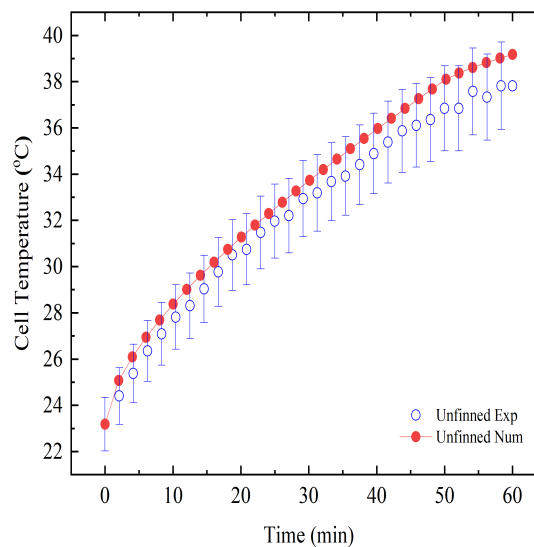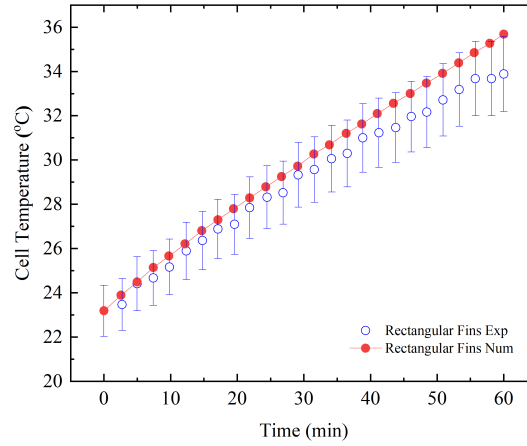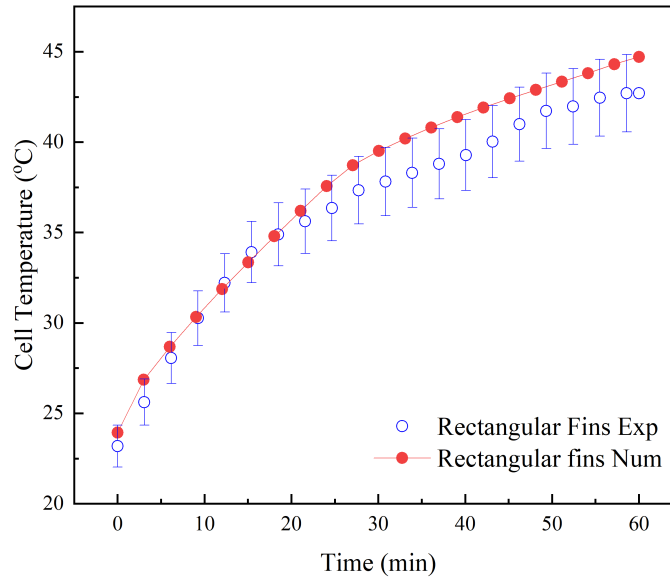

FIGURE 5.11: Comparison and validation of numerical prediction using experimental results for unfinned LIB pack at 3C discharge rate.

5.3.3   Heat Transfer in PCM at Different Discharge Rates

The temperature distribution and melt fraction evolution are shown in Figures 5.12 and Figure 5.13, which indicate that the temperature propagation for the rectangular fin case was higher compared to the unfinned case. The heat accumulation in the unfinned case at 45 min was due to the PCM having a melt fraction of 100% near the cell wall, which created a thermal barrier close to the wall due to the low thermal conductivity of the PCM.

The rectangular fin case had lower cell temperatures and less heat accumulation as the fins propagated the heat into the PCM, even if the PCM at the cell surface was melted, which kept the cell temperatures lower than those of cells without fins. The corresponding melt fractions are shown in the Figure 5.12. The PCM on the top surface of the cells melted faster than that at the height H of the cells, which led to the spread of the melt fraction and flow at the top surface.
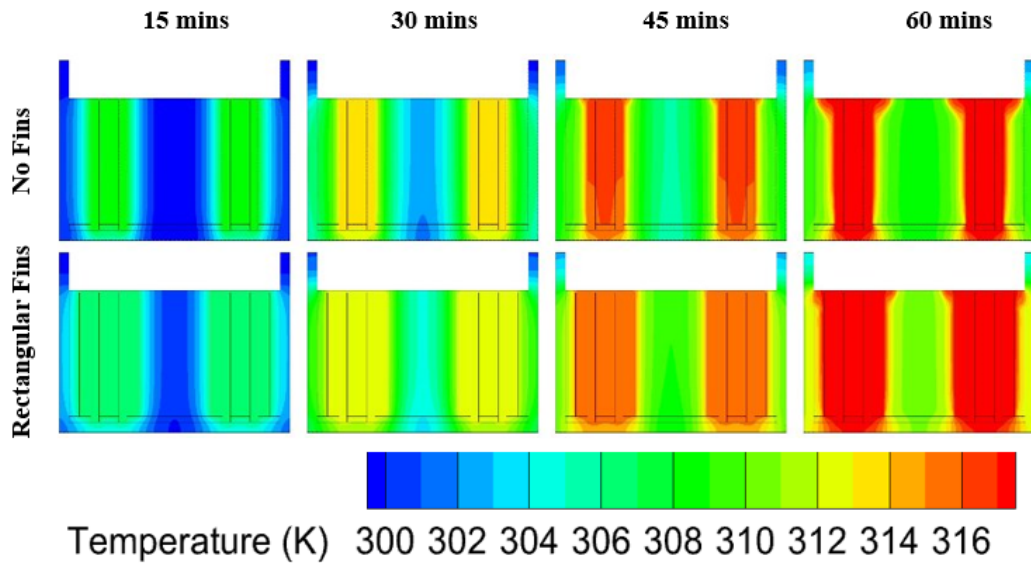
FIGURE 5.12: Temporal evolution of temperature for the unfinned and rectangular fin cases at the 3C discharge rate.
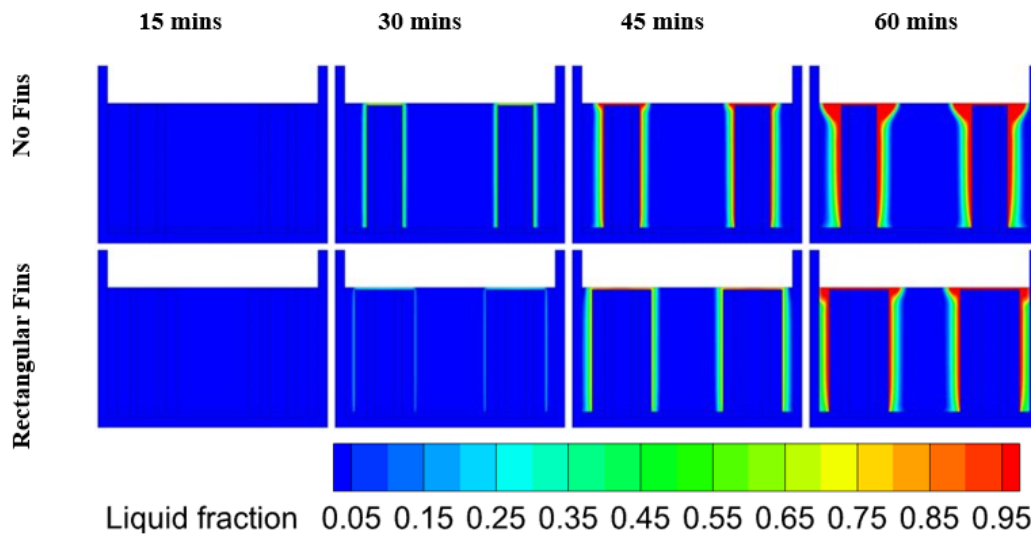
FIGURE 5.13: Temporal evolution of liquid fraction in the unfinned and rectangular fin cases, with the maximum melt fraction occurring at 60 min at the 3C discharge rate.

The temperature variation at the 2C discharge rate had a similar behavior as discussed in the 3C section. The temperature contours are shown in Figure 5.14. The temperature propagation is also depicted and it can be seen that heat from the acrylic housing was lost to the environment at free stream temperature with a heat transfer coefficient of 2.5 W/m²-K. The melting fraction in the unfinned and rectangular fin cases remained 0% as the melting was only localized on the cell top surface and close to the cell wall along the height of the cells. The overall melt
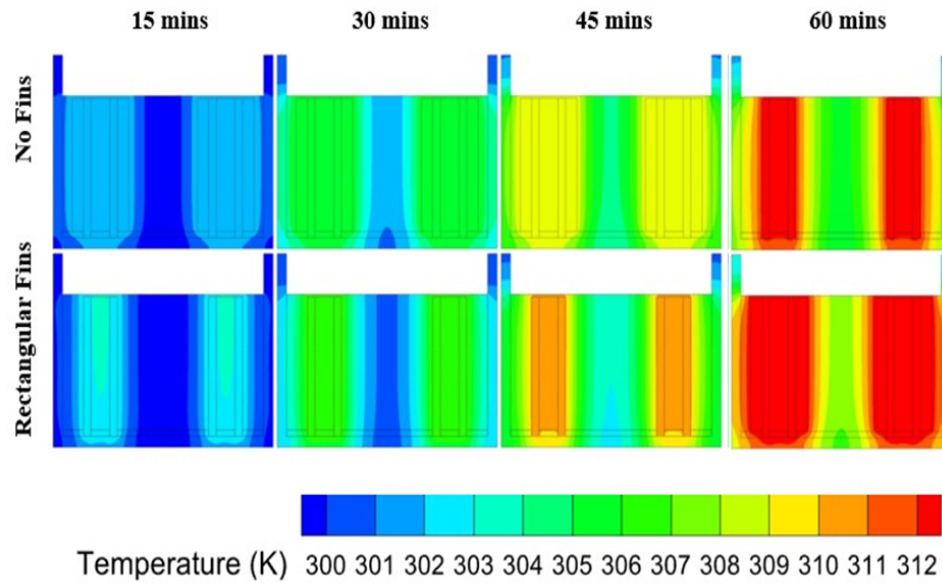
FIGURE 5.14: Temporal evolution of temperature for the unfinned and rectangular fin cases at the 2C discharge rate.
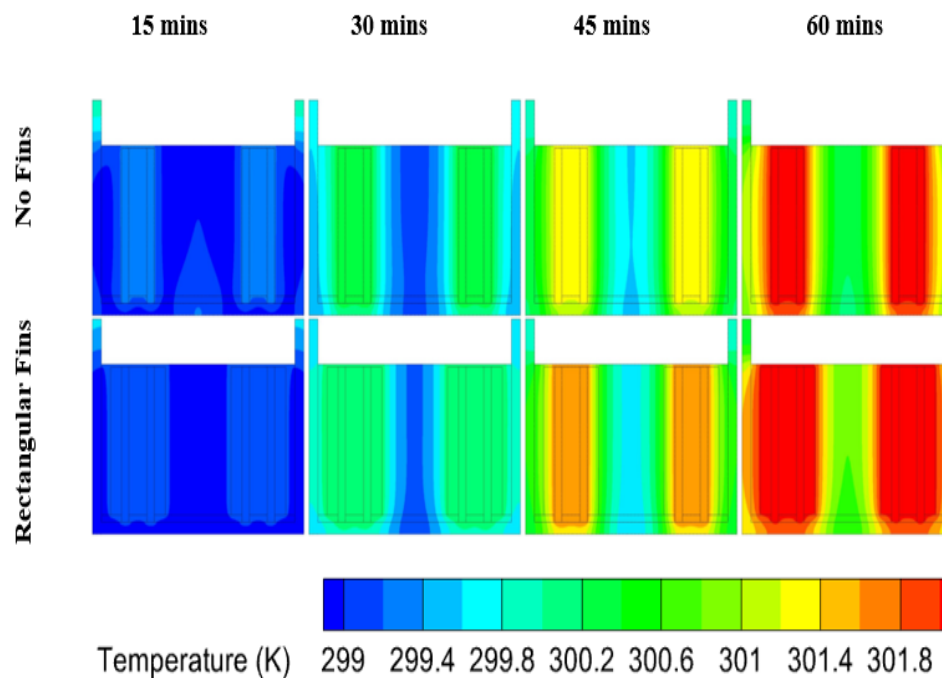
FIGURE 5.15: Temporal evolution of temperature for the unfinned and rectangular fin cases at the 1C discharge rate.

fraction reached a maximum value of 1.3% at 60 mins. The temperature contours for the 1C discharge rate are shown in Figure 5.15. The heating rate was very low, which can be seen clearly in the results. However, the rectangular fin case tended to dominate in performance, keeping the temperatures lower than those in the unfinned case.

5.4   Temporal Variation of Energy Storage Rate

The temporal variation depicted in Figure 5.16 illustrates the energy storage rate corresponding to various discharge rates for both the unfinned and Rectangular fins case. Notably, the energy storage rates for 1C and 2C discharge rates exhibit complete overlap in both cases. This phenomenon arises from their confinement within the conduction region, where no surface melting of the cell or fins occurs. Specifically, at a 1C discharge rate, the energy storage rate ranges from 0.99 W at t=5 mins to 0.45 W at t=60 mins, while at 2C, it varies between 1.6 W and 1.4 W during the same time intervals.

However, at a 3C discharge rate, the superiority of the Rectangular fins case over the unfinned case becomes apparent. Initially, both cases exhibit a similar trend until t=45 mins, with the unfinned case maintaining dominance. Beyond this point, the enhanced heat propagation facilitated by the fins enables the Rectangular fins case to surpass the unfinned case.

At t=60 mins, the Rectangular fins case achieves a maximum energy storage rate of 5.9 W, demonstrating the significant impact of fins on enhancing heat dissipation and thereby improving energy storage performance over time.
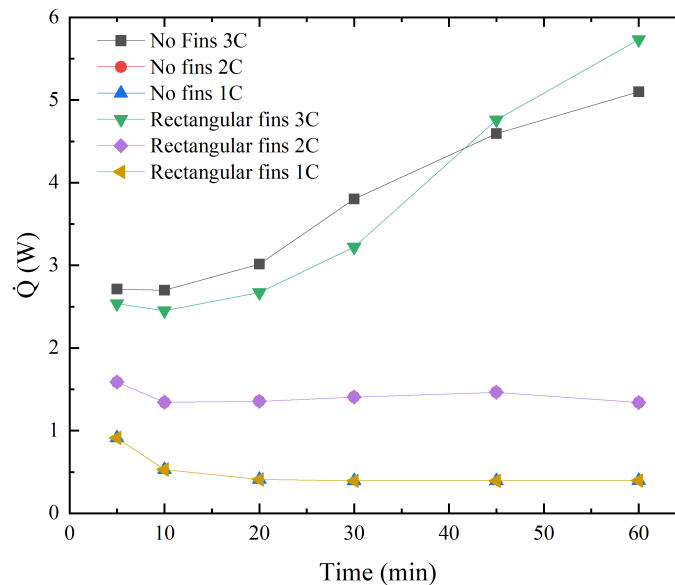
FIGURE 5.16: Variation in energy storage rate in the PCM at different discharge rates for unfinned and rectangular fins cases.

5.5 Average Nusselt Number and Heat Transfer Coefficient Variations

The heat transfer coefficient could be calculated using the energy stored in the PCM from the simulations. The values obtained for energy (J/kg) were multiplied by the mass of the PCM used in the system and by the flow time at that data point. The following mathematical formulation was used to calculate the heat transfer coefficient and Nusselt number:

$$\dot{Q}(t) = \frac{Q\,(\text{J/kg}) \cdot m\,(\text{kg})}{t\,(\text{s})} \tag{5.2}$$

The heat transfer coefficient was obtained from

$$\dot{Q}(t) = hA_s(T_{\text{pcm}}(t) - T_{\text{pcm,ref}}) \tag{5.3}$$

$$h(t) = \frac{\dot{Q}(t)}{A_s(T_{\text{pcm}}(t) - T_{\text{pcm,ref}}(t=0))} \quad (\text{W/(m}^2\text{-K})) \tag{5.4}$$

where $T_{\text{pcm}}(t)$ is the temperature of the PCM at a specific timestep (flow time) and $T_{(\text{pcm, ref}(t=0))}$ is the reference PCM temperature. The heat transfer coefficient could then be further used to calculate the Nusselt number for each case at the 1C, 2C, and 3C discharge rates.

$$Nu = \frac{hL}{\lambda} \tag{5.5}$$

where h is the heat transfer coefficient, L is the characteristic dimension (which was the height H of the cell in this case), and λ is the thermal conductivity of the PCM. The Nusselt numbers were then calculated for each timestep and averaged for each case to compare the convection to the diffusion. The average Nusselt numbers are shown in Figure 5.17, which indicate that the convective heat transfer of the PCM was stronger in the rectangular fin case due to the propagating heat transfer into the PCM compared to the unfinned case, where heat propagation slowed down as soon as the PCM around the cell melted and the localized temperature rise caused the PCM to melt only around the cell surface.
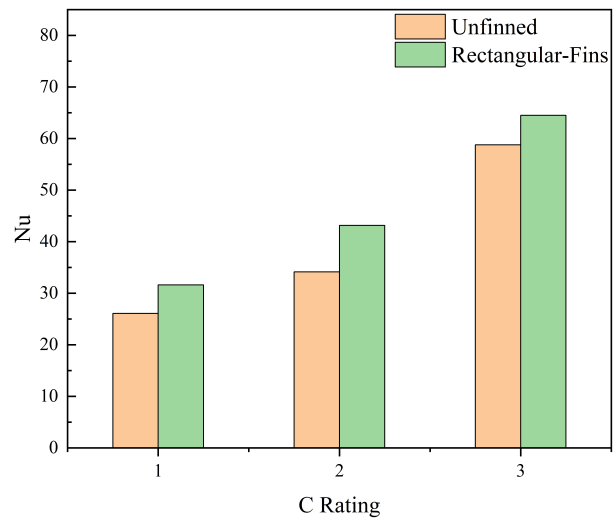
FIGURE 5.17: Average Nusselt number variations with C rating, averaged for different timesteps for comparison.

Chapter 6

Conclusion and Future Work

Conclusion

The thermal performance of a 2×2 li-ion battery pack was enhanced using the passive cooling method. The PCM RT-42 was highly effective compared to the system being placed in natural convection. The performance of the system was further investigated and enhanced by introducing fins on the external surfaces of the cells. It is pertinent to mention that the effective surface area and mass of the PCM were kept constant for all cases. The important conclusions are presented below:

1. The thermal performance at the 3C discharge rate for the unfinned case placed in natural convection compared to being placed in the PCM had a temperature enhancement of 9.44% at the time endpoint, while the naturally cooled system reached 40 °C at 5.6 min and the system placed in the PCM reached 40 °C at 28.42 min, which showed an enhancement in operating time of 185%;

2. The optimal rectangular fin case produced the lowest temperatures at 60 min, which produced an operating time enhancement of 34.17% over the unfinned case, while the temperature enhancement for a 60-min cycle was 6.91%;

3. During a complete cycle of 60 min, most of the cases exceeded the optimal cell temperature as heat accumulated due to the PCM having low thermal conductivity;

4. Cases at the 1C and 2C discharge rates did not exceed the optimum cell temperature and the PCM remained in the conduction region for all the cases except the unfinned case;

5. An improvement in Nusselt number of 9.72% at 3C, 20% at 2C and 15.63% at 1C was observed when the rectangular fin and unfinned cases were compared.

Future Work

The results achieved in this study lead to more research openings where a number of perspectives regarding the effective and efficient thermal performance enhancement can be studied. In the future work:

1. The PCM thickness around the cells and pitch of the cell in the LIB pack optimization is a critical perspective to reduce the Lithium-Ion Battery Pack weight, which is a very critical parameter during application in electric vehicles.

2. The current study takes into account only 1C, 2C and 3C discharge rates, however the Lithium-Ion cells can run at higher discharge rates depending on their geometry and construction of anode and cathode. Studying a single cell at higher discharge rates is the current goal.

3. The effect of orientation of the battery pack at different angles as well as in the horizontal direction is also a critical parameter which needs to be studied.

4. The effect of fin orientation and number of fins optimization and could be studied experimentally.

5. The PCM having low thermal conductivity is a problem for implementation of the passive cooling in BTMS. Currently, the author is working on development and optimization of nanoparticles enhanced RT-42 paraffin wax using Carbon Nano Tubes (CNTs). It is a work in progress where the composite PCM is developed and is being characterized. The results might show that due to a drastic improvement in the thermal conductivity, the fin geometry introduction might not be required.

Bibliography

[1] M. K. Rathod, "Thermal stability of phase change material," in *Phase Change Materials and Their Applications* (M. Mhadhbi, ed.), ch. 3, Rijeka: IntechOpen, 2018.

[2] C. C. Chan, "The state of the art of electric and hybrid vehicles," *Proceedings of the IEEE*, vol. 90, no. 2, pp. 247–275, 2002.

[3] C.-F. Chiasserini and R. R. Rao, "Energy efficient battery management," *IEEE journal on selected areas in communications*, vol. 19, no. 7, pp. 1235–1245, 2001.

[4] F. Meng, L. Chen, and Z. Xie, "Numerical simulations and analyses on thermal characteristics of 18650 lithium-ion batteries with natural cooling conditions," *International Journal of Energy and Environment*, vol. 8, no. 1, p. 43, 2017.

[5] S. Panchal, I. Dincer, M. Agelin-Chaab, R. Fraser, and M. Fowler, "Thermal modeling and validation of temperature distributions in a prismatic lithium-ion battery at different discharge rates and varying boundary conditions," *Applied Thermal Engineering*, vol. 96, pp. 190–199, 2016.

[6] S. Panchal, I. Dincer, M. Agelin-Chaab, R. Fraser, and M. Fowler, "Experimental and theoretical investigation of temperature distributions in a prismatic lithium-ion battery," *International Journal of Thermal Sciences*, vol. 99, pp. 204–212, 2016.

[7] R. Quadrelli and S. Peterson, "The energy–climate challenge: Recent trends in co2 emissions from fuel combustion," *Energy policy*, vol. 35, no. 11, pp. 5938–5952, 2007.

[8] G. Zhou, X. Ou, and X. Zhang, "Development of electric vehicles use in china: A study from the perspective of life-cycle energy consumption and greenhouse gas emissions," *Energy Policy*, vol. 59, pp. 875–884, 2013.

[9] M. Spiller, G. Rancilio, F. Bovera, G. Gorni, S. Mandelli, F. Bresciani, and M. Merlo, "A model-aware comprehensive tool for battery energy storage system sizing," *Energies*, vol. 16, no. 18, 2023.

[10] M. S. Hosen, R. Youssef, T. Kalogiannis, J. Van Mierlo, and M. Berecibar, "Battery cycle life study through relaxation and forecasting the lifetime via machine learning," *Journal of Energy Storage*, vol. 40, p. 102726, 2021.

[11] L. Lu, X. Han, J. Li, J. Hua, and M. Ouyang, "A review on the key issues for lithium-ion battery management in electric vehicles," *Journal of power sources*, vol. 226, pp. 272–288, 2013.

[12] R. Youssef, M. S. Hosen, J. He, J. Jaguemont, M. Akbarzadeh, L. De Sutter, J. Van Mierlo, and M. Berecibar, "Experimental and numerical study on the thermal behavior of a large lithium-ion prismatic cell with natural air convection," *IEEE Transactions on Industry Applications*, vol. 57, no. 6, pp. 6475–6482, 2021.

[13] J. Kim, J. Oh, and H. Lee, "Review on battery thermal management system for electric vehicles," *Applied thermal engineering*, vol. 149, pp. 192–212, 2019.

[14] J. R. Patel and M. K. Rathod, "Recent developments in the passive and hybrid thermal management techniques of lithium-ion batteries," *Journal of Power Sources*, vol. 480, p. 228820, 2020.

[15] T. Yang, N. Yang, X. Zhang, and G. Li, "Investigation of the thermal performance of axial-flow air cooling for the lithium-ion battery pack," *International Journal of Thermal Sciences*, vol. 108, pp. 132–144, 2016.

[16] W. Wu, S. Wang, W. Wu, K. Chen, S. Hong, and Y. Lai, "A critical review of battery thermal performance and liquid based battery thermal management," *Energy conversion and management*, vol. 182, pp. 262–281, 2019.

[17] Q. Wang, B. Jiang, Q. Xue, H. Sun, B. Li, H. Zou, and Y. Yan, "Experimental investigation on ev battery cooling and heating by heat pipes," *Applied Thermal Engineering*, vol. 88, pp. 54–60, 2015.

[18] J. Jaguemont, N. Omar, P. Van den Bossche, and J. Mierlo, "Phase-change materials (pcm) for automotive applications: A review," *Applied thermal engineering*, vol. 132, pp. 308–320, 2018.

[19] S. Ali and M. M. Khan, "Experimental investigation of battery thermal management system of lithium-ion cells using pcm," *Engineering Proceedings*, vol. 45, no. 1, p. 52, 2023.

[20] X. Lin, H. Fu, H. E. Perez, J. B. Siege, A. G. Stefanopoulou, Y. Ding, and M. P. Castanier, "Parameterization and observability analysis of scalable battery clusters for onboard thermal management," *Oil & Gas Science and Technology–Revue d'IFP Energies nouvelles*, vol. 68, no. 1, pp. 165–178, 2013.

[21] H. Teng, Y. Ma, K. Yeow, and M. Thelliez, "An analysis of a lithium-ion battery system with indirect air cooling and warm-up," *SAE International Journal of Passenger Cars-Mechanical Systems*, vol. 4, no. 2011-01-2249, pp. 1343–1357, 2011.

[22] C. G. Motloch, J. P. Christophersen, J. R. Belt, R. B. Wright, G. L. Hunt, R. A. Sutula, T. Duong, T. J. Tartamella, H. J. Haskins, and T. J. Miller, "High-power battery testing procedures and analytical methodologies for hev's," *SAE Transactions*, pp. 797–802, 2002.

[23] R. Sabbah, R. Kizilel, J. Selman, and S. Al-Hallaj, "Active (air-cooled) vs. passive (phase change material) thermal management of high power lithium-ion packs: Limitation of temperature rise and uniformity of temperature distribution," *Journal of power sources*, vol. 182, no. 2, pp. 630–638, 2008.

[24] Y. Wei and M. Agelin-Chaab, "Development and experimental analysis of a hybrid cooling concept for electric vehicle battery packs," *Journal of Energy Storage*, vol. 25, p. 100906, 2019.

[25] S. Park and D. Jung, "Battery cell arrangement and heat transfer fluid effects on the parasitic power consumption and the cell temperature distribution in a hybrid electric vehicle," *Journal of Power Sources*, vol. 227, pp. 191–198, 2013.

[26] D. R. Pendergast, E. P. DeMauro, M. Fletcher, E. Stimson, and J. C. Mollendorf, "A rechargeable lithium-ion battery module for underwater use," *Journal of Power Sources*, vol. 196, no. 2, pp. 793–800, 2011.

[27] G. Xia, L. Cao, and G. Bi, "A review on battery thermal management in electric vehicle application," *Journal of power sources*, vol. 367, pp. 90–105, 2017.

[28] Y. Huo and Z. Rao, "The numerical investigation of nanofluid based cylinder battery thermal management using lattice boltzmann method," *International Journal of Heat and Mass Transfer*, vol. 91, pp. 374–384, 2015.

[29] M. Al-Zareer, I. Dincer, and M. A. Rosen, "Electrochemical modeling and performance evaluation of a new ammonia-based battery thermal management system for electric and hybrid electric vehicles," *Electrochimica acta*, vol. 247, pp. 171–182, 2017.

[30] M. Al-Zareer, I. Dincer, and M. A. Rosen, "Novel thermal management system using boiling cooling for high-powered lithium-ion battery packs for hybrid electric vehicles," *Journal of power sources*, vol. 363, pp. 291–303, 2017.

[31] S. Al Hallaj and J. Selman, "A novel thermal management system for electric vehicle batteries using phase-change material," *Journal of the Electrochemical Society*, vol. 147, no. 9, p. 3231, 2000.

[32] R. D. Jilte, R. Kumar, M. H. Ahmadi, and L. Chen, "Battery thermal management system employing phase change material with cell-to-cell air cooling," *Applied Thermal Engineering*, vol. 161, p. 114199, 2019.

[33] F. Chen, R. Huang, C. Wang, X. Yu, H. Liu, Q. Wu, K. Qian, and R. Bhagat, "Air and pcm cooling for battery thermal management considering battery cycle life," *Applied Thermal Engineering*, vol. 173, p. 115154, 2020.

[34] Z. Wang, H. Zhang, and X. Xia, "Experimental investigation on the thermal behavior of cylindrical battery with composite paraffin and fin structure," *international journal of heat and mass transfer*, vol. 109, pp. 958–970, 2017.

[35] Z. Sun, R. Fan, F. Yan, T. Zhou, and N. Zheng, "Thermal management of the lithium-ion battery by the composite pcm-fin structures," *International Journal of Heat and Mass Transfer*, vol. 145, p. 118739, 2019.

[36] Y. Zhao, B. Zou, C. Li, and Y. Ding, "Active cooling based battery thermal management using composite phase change materials," *Energy Procedia*, vol. 158, pp. 4933–4940, 2019.

[37] J. Weng, D. Ouyang, X. Yang, M. Chen, G. Zhang, and J. Wang, "Experimental study on thermal behavior of pcm-module coupled with various cooling strategies under different temperatures and protocols," *Applied Thermal Engineering*, vol. 197, p. 117376, 2021.

[38] P. Goli, S. Legedza, A. Dhar, R. Salgado, J. Renteria, and A. A. Balandin, "Graphene-enhanced hybrid phase change materials for thermal management of li-ion batteries," *Journal of Power Sources*, vol. 248, pp. 37–43, 2014.

[39] L. Ghadbeigi, B. Day, K. Lundgren, and T. D. Sparks, "Cold temperature performance of phase change material based battery thermal management systems," *Energy Reports*, vol. 4, pp. 303–307, 2018.

[40] M. Ramandi, I. Dincer, and G. Naterer, "Heat transfer and thermal management of electric vehicle batteries with phase change materials," *Heat and mass transfer*, vol. 47, pp. 777–788, 2011.

[41] Z. Jiang and Z. Qu, "Lithium–ion battery thermal management using heat pipe and phase change material during discharge–charge cycle: A comprehensive numerical study," *Applied Energy*, vol. 242, pp. 378–392, 2019.

[42] W. Li, Z. Qu, Y. He, and Y. Tao, "Experimental study of a passive thermal management system for high-powered lithium ion batteries using porous metal foam saturated with phase change materials," *Journal of power sources*, vol. 255, pp. 9–15, 2014.

[43] R. Nasehi, A. Alamatsaz, and M. R. Salimpour, "Using multi-shell phase change materials layers for cooling a lithium-ion battery," *Thermal Science*, vol. 20, no. 2, pp. 391–403, 2016.

[44] N. O. Moraga, J. P. Xamán, and R. H. Araya, "Cooling li-ion batteries of racing solar car by using multiple phase change materials," *Applied Thermal Engineering*, vol. 108, pp. 1041–1054, 2016.

[45] M. Safdari, R. Ahmadi, and S. Sadeghzadeh, "Numerical investigation on pcm encapsulation shape used in the passive-active battery thermal management," *Energy*, vol. 193, p. 116840, 2020.

[46] Y. Li, Y. Du, T. Xu, H. Wu, X. Zhou, Z. Ling, and Z. Zhang, "Optimization of thermal management system for li-ion batteries using phase change material," *Applied Thermal Engineering*, vol. 131, pp. 766–778, 2018.

[47] Z. Rao, Q. Wang, and C. Huang, "Investigation of the thermal performance of phase change material/mini-channel coupled battery thermal management system," *Applied energy*, vol. 164, pp. 659–669, 2016.

[48] W. Wu, X. Yang, G. Zhang, K. Chen, and S. Wang, "Experimental investigation on the thermal performance of heat pipe-assisted phase change material based battery thermal management system," *Energy Conversion and Management*, vol. 138, pp. 486–492, 2017.

[49] Z. An, X. Chen, L. Zhao, and Z. Gao, "Numerical investigation on integrated thermal management for a lithium-ion battery module with a composite phase change material and liquid cooling," *Applied Thermal Engineering*, vol. 163, p. 114345, 2019.

[50] M. Shojaeefard, G. Molaeimanesh, and Y. S. Ranjbaran, "Improving the performance of a passive battery thermal management system based on pcm using lateral fins," *Heat and Mass Transfer*, vol. 55, pp. 1753–1767, 2019.

[51] R. Youssef, M. S. Hosen, J. He, A.-S. Mohammed, J. Van Mierlo, and M. Berecibar, "Novel design optimization for passive cooling pcm assisted battery thermal management system in electric vehicles," *Case Studies in Thermal Engineering*, vol. 32, p. 101896, 2022.

[52] R. Huang, Z. Li, W. Hong, Q. Wu, and X. Yu, "Experimental and numerical study of pcm thermophysical parameters on lithium-ion battery thermal management," *Energy Reports*, vol. 6, pp. 8–19, 2020.

[53] M. M. El Idi, M. Karkri, and M. A. Tankari, "A passive thermal management system of li-ion batteries using pcm composites: Experimental and numerical investigations," *International Journal of Heat and Mass Transfer*, vol. 169, p. 120894, 2021.

[54] X. Duan and G. Naterer, "Heat transfer in phase change materials for thermal management of electric vehicle battery modules," *International Journal of Heat and Mass Transfer*, vol. 53, no. 23-24, pp. 5176–5182, 2010.

[55] C.-V. Hémery, F. Pra, J.-F. Robin, and P. Marty, "Experimental performances of a battery thermal management system using a phase change material," *Journal of Power Sources*, vol. 270, pp. 349–358, 2014.

[56] S. A. Khateeb, M. M. Farid, J. R. Selman, and S. Al-Hallaj, "Design and simulation of a lithium-ion battery with a phase change material thermal management system for an electric scooter," *Journal of power sources*, vol. 128, no. 2, pp. 292–307, 2004.

[57] V. Choudhari, A. Dhoble, and S. Panchal, "Numerical analysis of different fin structures in phase change material module for battery thermal management system and its optimization," *International Journal of Heat and Mass Transfer*, vol. 163, p. 120434, 2020.

[58] V. R. Voller and C. Prakash, "A fixed grid numerical modelling methodology for convection-diffusion mushy region phase-change problems," *International journal of heat and mass transfer*, vol. 30, no. 8, pp. 1709–1719, 1987.

[59] A. Olabi, H. M. Maghrabie, O. H. K. Adhari, E. T. Sayed, B. A. Yousef, T. Salameh, M. Kamil, and M. A. Abdelkareem, "Battery thermal management systems: Recent progress and challenges," *International Journal of Thermofluids*, vol. 15, p. 100171, 2022.